

EXPERIMENTAL AND NUMERICAL INVESTIGATION OF POOL BOILING HEAT TRANSFER FROM FINNED SURFACES

Rajan Jaswal[1], A. Sathyabhama[1*], Kuldeep Singh[2], A.V.V.R. Prasad Yandapalli[1]

[1]Department of Mechanical Engineering, National Institute of Technology Karnataka, Surathkal, Mangalore, India, 575025.
[2]Faculty of Engineering, University of Nottingham, UK
*Corresponding author email: bhama72@gmail.com

ABSTRACT

An experimental study of the pool boiling process on three test surfaces, namely, Plain surface, Rectangular finned surface, and Trapezoidal finned surface, was carried out using distilled water as the working fluid at atmospheric pressure. A parametric study of finned surfaces was performed to understand the effect of fin spacing and fin height on the pool boiling performance. A high-speed camera was employed to capture the pool boiling process. A numerical investigation was also performed using the Eulerian multiphase model associated with the RPI wall boiling model. A 2-D rectangular boiling chamber filled with distilled water was considered for the numerical study. The numerical results with default models were validated with the experimental results. A correction was proposed for the Bubble Waiting Time coefficient (C_w) of the quenching heat flux to improve the numerical results. Experimental results showed that using rectangular and trapezoidal finned surfaces improved the heat flux values by 52.3% and 101.5%, respectively, compared to the plain surface. The heat transfer coefficient (HTC) depends upon the area availability and type of boiling surface used. Increasing the height of the fins was beneficial, whereas increasing the fin spacing adversely affected the fin performance.

Keywords: Pool boiling, fins, Eulerian model, Bubble waiting time coefficient (C_w), Heat transfer

NOMENCLATURE

A	contact area (m^2)
C_D	drag coefficient
C_l, C_{TD}	coefficient appeared in phase interaction
C_w	quenching bubble waiting time coefficient
C_{WL}	wall lubrication coefficient
$C_\mu, \sigma_k, \sigma_\varepsilon, C_{\varepsilon1}, C_{\varepsilon2}$	constants in the turbulence model

d_{bubble}	bubble departure diameter (mm)
dT/dx	temperature gradient (K/m)
E	energy (J)
f	bubble departure frequency (1/s)
F_{LW}	wall lubrication force (N)
g	acceleration due to gravity (m/s^2)
h_{lg}	latent heat of vaporization (kJ/kg)
h	heat transfer coefficient (kJ/kg K)
K	turbulent kinetic energy (J)
K	thermal conductivity (W/mK)
$\dot{m}$	mass flow rate (kg/s)
N_a	active nucleation site density (sites/cm^2)
Nu	Nusselt number
P	pressure (Pa)
Pr	Prandtl number
q	heat flux (W/m^2)
Re	Reynolds number
S	source term
T_s	surface temperature (K)
T_{sat}	saturation temperature (K)
T_w	wall temperature (K)
t	time (s)
t_w	waiting time period (s)
V	Volume (m^3)
V	Velocity (m/s)

Greek symbol		**Subscript**	
α	volume fraction (%)	L	liquid
μ	viscosity (Pa-s)	G	gas
ρ	density (kg/m^3)	evap.	evaporative
σ	surface tension (N/m)	conv	convective
ε	turbulence dissipation rate (m^2/s^3)	quen.	quenching
ΔT	wall superheat (K)	K	fluid
		Sup	superheat

Abbreviation

HTC	heat transfer coefficient
CHF	critical heat flux
CFD	computational fluid dynamics
PS	plain surface
RF	rectangular finned surface
TF	trapezoidal finned surface
HFP	heat flux partitioning

1. INTRODUCTION

In the last decade, the advancement in the field of engineering and technology resulted in the upgradation of instruments and equipment. Due to this, the functionality of devices has improved along with the decrease in size and weight. Compact devices face the problem of high heat load, and this limits their efficiency. Inefficient cooling in these devices not only affects the performance but can also decrease the life span of the device. This indicates that an efficient cooling system is required. Traditional air cooling or single-phase cooling systems are inefficient in fulfilling the heat transfer requirement of devices like advanced microchips, hybrid electric vehicles, fuel cells, aircraft and spacecraft, advanced radar, etc. Two-phase cooling, such as pool boiling, was a better option than single-phase cooling systems for heat transfer in advanced devices.

The pool boiling process is a very complex phenomenon, and a lot of research is going on to understand the concept of pool boiling heat transfer. The critical heat flux (CHF) value determines the maximum heat transfer possible in the nucleate pool boiling process under a given condition. Most of the research related to pool boiling focused on increasing the value of CHF and pool boiling heat transfer coefficient. It is very difficult to site a particular set of conditions to achieve a higher CHF value, as pool boiling heat transfer depends on many parameters such as operating pressure, type of working fluid, the structure of the heated surface, surface tension between heated surface and the working liquid, surface roughness, etc. The effect of operating pressure on boiling heat transfer was studied by Barthua (1992). He carried out an experiment at a range of 1.5 bar to 2.47 bar with R114 as a working medium. Results showed that the number of nucleation sites increased with increasing operating pressure, but the contribution of individual sites decreased. Moreover, the average distance between nucleation sites was equal to the bubble departure diameter.

Different methods are available to enhance pool boiling heat transfer, broadly categorized as passive and active. In the passive method, the focus is on improving or optimizing the heated surface and properties of the working liquid. The surface area of the heater can be enhanced by using fins, grooves, microchannels, and porous structures. On the other hand, the active method involves external energy sources like an electric field or surface vibration to improve the performance of the pool boiling process. Wei et al. (2020) reviewed different active and passive methods used in the past for boiling heat transfer enhancement. They presented passive methods like structured surface, heterogeneous wettability surface, and coated surface. All these methods tend to delay CHF value, so pool boiling heat transfer was increased. An active method included smart surfaces like shape memory alloy, switchable polymer coating, metal oxide film, etc. But they also highlighted some challenges related to these methods, like difficulty in fabricating structured surfaces, peel-off coating from the surface, and passive surfaces performing well at specified boiling conditions.

Structured surface in pool boiling is the most studied research topic. Using a structured surface increases the surface area and modifies the bubble formation and departure mechanism in pool boiling. Jiang et al. (2021) performed a pool boiling experiment on a plain surface and surfaces with a cylindrical array of different dimensions at atmospheric conditions. The result showed that the onset of nucleate boiling temperature decreases in the case of the structured surface. Moreover, the heat transfer coefficient (HTC) was increased by 23.4% - 163.4% compared to the smooth surface. A decrease in pillar gap leads to increased liquid capillary action and easy liquid replenishment at dried places. There are many research papers related to the parametric study of fins of different shapes in the pool boiling process. Yu et al. (2007) presented the flow pattern and pool boiling heat transfer performance of rectangular copper finned array immersed in FC-72. They examined workpieces of three different fin spacings (0.5mm, 1mm, 2mm) and four fin lengths (0.5mm,1mm, 2mm, 4mm). The result indicated that higher fins provided resistance to bubble departure. Also, the workpiece with smaller fin spacing and higher fin height had a heat transfer rate of 5 times that of a plain surface. Nirgude and Sahu (2017) conducted experiments on polished copper and structured surfaces in a pool of water and isopropyl. Here the effect of intersecting tunnel geometry was observed. The results confirmed an improvement in the boiling heat transfer of structured surfaces and the HTC increased by 250% for water and 150% for isopropyl compared to plain surfaces. In a recent experimental study, Zhang et al. (2022) investigated the pool boiling performance of heterogeneous micro-pillar surfaces in FC-72 liquid maintained at different subcooled temperatures. They used six surfaces including three single block micro pillars (MS-1, MS-2, and MS-3) and three, four block micro pillar surfaces (BS-1, BS-2, and BS-3) which were fabricated by dry etching process. Results demonstrated that CHF was dependent on area enhancement ratio at high subcooled temperatures. Out of all surfaces, the BS-1 surface had the highest CHF improvement, nearly 1.57-2.05 times that of the plain surface and the HTC of MS-1 increased by 20% compared to the BS-2 surface. Moreover, the maximum HTC enhancement ratio was constant for higher subcooled temperatures (ΔT_{sub}> 15K).

Apart from traditional shapes of fins like rectangular and cylindrical, some researchers examined the fins like Y-shaped fins, T-shaped fins, parabolic fins, stepped fins, etc. One such experimental study was carried out by Hubner et al. (1997), investigating the performance of trapezoidal fins, T-shaped fins, and Y-shaped fins with different refrigerant liquids. They also modified the roughness of the trapezoidal fin by emery grinding and sandblasting. With the application of trapezoidal fins, pool boiling performance was enhanced. But a significant improvement was observed in the T-shaped fins and Y-shaped fins. However, some researchers used micro-channeled surfaces instead of fins on the surface for heat transfer enhancement. Avdhoot and Sathyabhama (2018) considered three different microchannel geometry: rectangular, parabolic, and stepped microchannel. They studied the performance of microchannel in distilled water with variation in the top and bottom width of the channel and variation in fin tip thickness. It was observed that liquid supply improved in the stepped microchannel due to the wider channel width at the top. The heat transfer rate of the rectangular microchannel increased by 182.8% compared to the plain surface. Moreover, there was an improvement of 38.6% and 169% in the case of parabolic and stepped microchannels compared with rectangular microchannels at 11.7℃ wall superheat. Zhang et al. (2023) conducted a subcooled pool boiling experiment utilizing hybrid surfaces created by sintering spherical copper powder onto mini-channels, with HFE-7100 serving as the working fluid. They observed that the ring groove around the mini-channels and capillary wick had a significant effect on the boiling heat transfer due to a larger number of nucleation sites. The maximum CHF for hybrid surfaces coupling capillary wick and the mini channel was reported to be 147.4 W/cm^2, along with 2.69 $W/cm^2.K$ as the HTC. Apart from this, 86.8% and 192% improvements were recorded in CHF and HTC values of mini channels without a capillary wick.

Researchers have recently started performing numerical investigations of the pool boiling heat transfer process. Modelling the pool boiling process in the numerical study is an arduous task due to the dependence of pool boiling on various parameters like nucleation site density, bubble departure diameter, bubble departure frequency, pressure, area of influence, drag, lift force, etc. Multiphase models like the Eulerian, VOF, and Mixture models are available for numerical simulation of pool boiling heat transfer. Each multiphase model has pros and cons, and the model selection depends on the problem definition. To understand the difference between the Eulerian model and the VOF model, a comparative study was performed by Guerrero et al. (2017). They employed Eulerian and VOF models to assess two-phase flow in the vertical pipes. Results demonstrated that the performance of the Eulerian model was independent of grid quality, whereas VOF showed dependence on grid size. The accuracy of the Eulerian model was higher as compared to the VOF model, but the Eulerian model required more simulation time. Of these two models, only the VOF model successfully presented a flow pattern of continuous and discontinuous phases of two-phase flow. Zhao et al. (2017) used the VOF method to study the pool boiling performance of surfaces combining microstructures and different wetting properties. They considered different two-dimensional (2-D) surfaces like flat and micro-structured surfaces with hydrophilic wetting properties and flat and micro-structure surfaces with mixed hydrophilic and hydrophobic wetting properties. The effect of variation in height and width of microstructure was also studied in this paper. Results showed that hydrophilic flat surfaces had better bubble departure frequency, bubble departure speed, HTC, and lower temperature than hydrophilic flat with hydrophobic spots. The temperature of a heated surface consisting of hydrophilic microstructure and hydrophilic microstructure with hydrophobic spots was reduced by 4.36% and 4.75%, respectively, compared to flat surface temperature. Moreover, HTC was also improved by increasing the height and width of the microstructure.

Modeling two-phase gas-liquid flow using computational tools is challenging because it involves many closure laws and correlations to be defined. More than generalized correlations, as utilized by computational tools, may be required to capture the physical behavior accurately. Thus, the success of modelling depends on the accuracy of the correlations. Montoya et al. (2019) investigated different interfacial closure laws, heat and mass transfer models, wall boiling models, bubble breakup and coalescence, and turbulence modelling. They discussed the applicability of various drag and non-drag force models available in ANSYS FLUENT and CFX, and the result was validated with experimental data. Non-drag forces mainly consist of lift, wall lubrication, turbulent dispersion, and virtual mass force. They observed that some modifications were required to apply drag models in FLUENT and CFX. Schiller – Naumann and Grace drag coefficient models gave similar results for FLUENT and CFX. But in the case of the lift coefficient model, FLUENT results were close to the experimental results.

Nanofluid is a new class of working fluid in thermal engineering. Nanofluid is a colloidal solution of nanoparticles of metals like copper, silver, aluminum oxide, zinc, etc., in base fluids like water, oil, ethylene glycol, etc. Kamel et al. (2020) presented the numerical study of pool boiling of nanofluid using the Eulerian multiphase model. They considered a 2-D pool boiling chamber filled with water and silica-based water nanofluid. They proposed a correlation of the bubble waiting time coefficient for water to validate the results with the experimental result. Apart from this, in the case of Silica-based nanofluid, correlation related to bubble departure diameter and nucleation site density was also presented to consider the change in surface roughness due to the deposition of nanoparticles. Results indicated that the volume fraction of water was higher than the nanofluid. Also, the HTC of water came out to be higher compared to nanofluid and it was observed that quenching heat flux played a major role in the pool boiling heat transfer process.

A numerical investigation of water and water–silica nanofluid in pool boiling heat transfer was performed by Salehi and Hormozi (2017). They used the classical heat flux partitioning model (HFP) to predict bubble parameters. There were nine cases of numerical simulation using different models of bubble departure frequency and nucleation site density. Results revealed that case number nine (using Hibiki Ishii and Hatton Hall Correlation) best agreed with the experimental result. They also observed that the wall temperature and the nucleation site density decreased at the edges, away from the center of the heater. This showed that heat transfer was due to evaporation at the center of the heater, whereas at the heater edge, it was through a convection process. Zhang et al. (2019) attempted to study the pool boiling performance of refrigerant R134a outside a plain tube at 279K & 299.7K as the saturation temperatures. The Eulerian multiphase model integrated with Rensselaer Polytechnic Institute (RPI) nucleate boiling model was adopted in this investigation. They validated numerical results with experimental results and observed a maximum deviation of 16%. To reduce the deviation between experimental and numerical results, they proposed modification in the exponent value of Lemmert and Chawla's model for higher and lower heat flux values. It was also observed that the volume fraction at the tube's end increased with saturation temperature. The region between 90º to 130º had the best heat transfer performance due to high velocity and turbulence. Farshad et al. (2021) used a numerical investigation to determine the pool boiling performance of the absorption chiller generator with different surfaces. In this paper, $\mathrm{LiBr/H_2O}$ was used as working fluid and three types of tube were considered for study – bare tube, tube with notched fins, and tube with low fins. Similar to the above works, they employed the Eulerian multiphase model but with an extended RPI nucleate boiling model. It was found that adding fins to the tube resulted in increased active nucleation site, bubble growth rate, bubble departure rate, and bubble merging rate. In the case of a low fin tube, the contact angle was high compared to a bare and notched fin tube, resulting in lower wettability and less boiling time.

Apart from nanofluids and refrigerants, some researchers were also interested in investigating cryogenics in the pool boiling heat transfer process. Chen et al. (2015) carried out both experimental and numerical investigations of liquid nitrogen (LN_2) performance in the pool boiling process. They employed the Eulerian multiphase model for numerical simulation. Results showed good agreement between experimental and numerical results. But numerical results were under-predicted using Tolubinsky and Kostanchuk, Lee et al. models for bubble departure diameter. So, to match experimental and numerical results, they proposed a correlation of bubble departure diameter as a function of Jacob number (Ja) in low heat flux region and fully developed nucleate boiling.

Enhancement of pool boiling can be done by either passive or active methods, but the combination of these two is also possible and termed the compound technique. The effect of this compound technique was studied by Alimoradi et al. (2021). They examined the pool boiling heat transfer performance of nanofluid with vibrating surfaces. They assumed nanofluid to be homogeneous as the concentration of nanoparticles was negligible. Results demonstrated an increase in boiling curve slope and HTC with the increase in the concentration of nanoparticles, amplitude, and frequency of vibration. They also proposed two correlations, one for HTC as a function of vibration amplitude and wall superheat and the second for nanofluid velocity as a function of vibration frequency. Wang et al. (2019) investigated the effect of upward and downward-facing hemispheres in pool boiling heat transfer. They considered the Eulerian model for numerical simulation. The reliability and accuracy of the numerical method were validated with experimental results. They observed that the modified heated surface had a higher heat flux value than the plain heated surface. In the case of the downward-facing hemisphere, the CHF value was lower than the upward-facing hemisphere. The modified heated surface provided more nucleation sites, increasing bubble coalescence. Buoyancy force also varied in modified surfaces, further enhancing bubble motion in pool boiling.

As detailed in the literature review above, there are numerous works on boiling heat transfer from modified surfaces. However, the size, orientation, fabrication method and other minute details are different in each work. The size and orientation of structures directly affect the bubble dynamics like bubble nucleation and departure, frequency and liquid rewetting, which may lead to different outcomes for each structured surface. Different studies were performed related to pool boiling performance with the finned surface also in literature, but very few data are available related to the pool boiling performance of the trapezoidal finned surface. On comparing trapezoidal fins with rectangular and cylindrical fins, we can observe that more surface area is available in the case of trapezoidal fins and the main reason for using fins is to enhance surface availability for heat transfer. Hence the pool boiling process on a trapezoidal finned surface is investigated experimentally and numerically and its performance is compared with that of the rectangular finned and plain test surface in the present work. Different multiphase models like Eulerian, VOF, and Mixture models are available in ANSYS FLUENT commercial software. The Eulerian model is the most complex multiphase model, and it solves n momentum and continuity equations for each phase. The VOF can model two or more immiscible fluids and solves only a single set of governing equations. The Mixture model mainly deals with particle-laden flows with low loading, sedimentation, and bubbly flow. In the pool boiling process, many bubbles nucleate from the test surface at a given instant of time. Still, the VOF model can only study one or two bubbles in the continuous fluid, due to which this model becomes computationally expensive for the numerical study of the pool boiling process. Apart from this, we cannot include interfacial interaction forces using the VOF model. However, the Eulerian model associated with the RPI model can model interaction forces between different phases and is computationally inexpensive. Along with this, the accuracy of the Eulerian model is higher in comparison to VOF multiphase model. Due to these reasons, the Eulerian multiphase model is selected to study the pool boiling process. Also, an effort is made in the present work to obtain practical results from the numerical simulations by modifying the default RPI boiling model. The modification involves the correction in Quenching Bubble Waiting Time Coefficient (C_w) and the correlations are proposed to determine the values of C_w for plain, rectangular finned and trapezoidal finned test surfaces at different wall superheat values. Saturated pool boiling at atmospheric pressure is considered and the heat flux value is evaluated for various parameters of fins.

1 METHODOLOGY

This section contains detailed information about the method followed during the experimental and numerical investigation of finned surfaces in the pool boiling process. In the experimental part, the specification of the pool boiling apparatus and its operating procedure are mentioned. Along with this, characteristics of the test surface and data reduction method are included here.

In the numerical study, computational geometry, the meshing of the computational domain, material properties, solver settings, and models employed are discussed.

2.1 Experimental Methodology

2.1.1 Pool Boiling Apparatus

Figure 1 shows the pool boiling apparatus used for the experimental study. It consists of a rectangular boiling chamber of dimensions 250×400×200 mm^3 made up of SS 304 fitted with SS 304 flange at the top and the bottom. Provisions for liquid charging, condenser cooling water inlet, and outlet are given on the top flange. The test section is inserted into the chamber through the bottom flange. The pressure transducer on the top flange indicates the chamber pressure. The vessel is fitted with three sight glasses to observe and capture the boiling phenomena. The copper condenser coil is connected to the cooling water tank through a pump and a PID. The water temperature (saturated) is maintained constant during experimentation by an auxiliary heater of 500 W capacity provided through the sidewall.

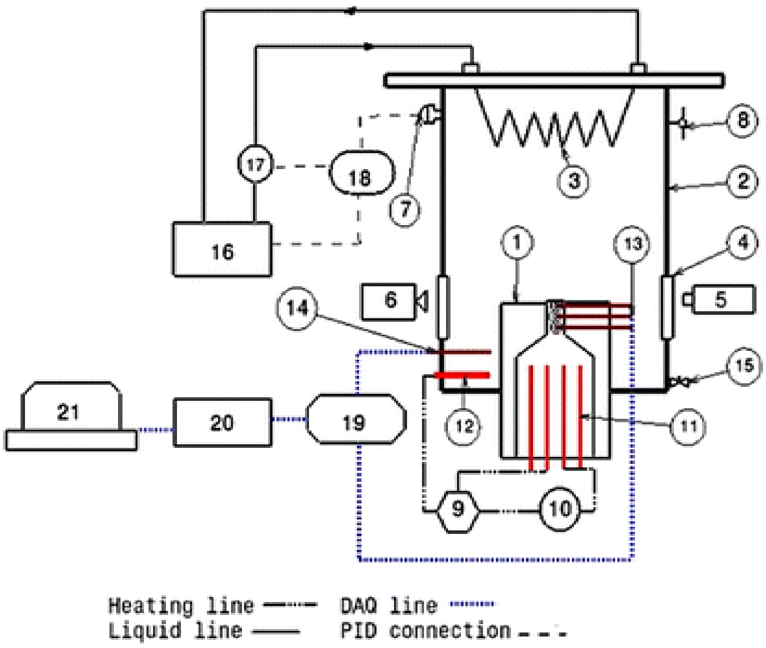

1	Test Section	8	PRV	15	Drain
2	Boiling Chamber	9	Main Supply	16	Water Tank
3	Condenser coil	10	Autotransformer	17	Pump
4	Sight glass	11	Main Cartridge Heaters	18	PID
5	CCD camera	12	Auxiliary Heater	19	Signal conditioner
6	Light source	13	Test Section Thermocouples	20	DAQ
7	Pressure sensor	14	Bulk Fluid Thermocouple	21	Workstation

Fig. 1 Schematic diagram of Pool Boiling Apparatus

The heater block and test surfaces are made of copper. Four high-density cartridge heaters with a capacity of 200W/230V can be facilitated from four holes provided at the bottom of the heater block. The cartridge heaters of 6 mm diameter and 50 mm length are connected in parallel to get maximum 800 W resultant heat input. For steady state observations, an incremental sample of heat supply is controlled by the autotransformer for approximately 10 minutes of the time interval.

A high-temperature Silicon Gasket and polytetrafluoroethylene tape are used to ensure leakproof assembly. A threaded joint ensures the air-tight fitting of a 20 mm thick replaceable copper circular test piece (ϕ=19 mm). Apart from this, the cylindrical wall of the test surface is provided with external threads to fit it into the internal threads of the Teflon insulation block that is provided to reduce heat losses in the radial direction. An arctic silver paste is applied over the joint for uniform temperature distribution across the diameter of the test piece and to reduce thermal contact resistance.

Three K-type SS 304 sheathed thermocouples of 1 mm diameter are planted at the centre of the test piece as 2 mm, 6 mm, and 10 mm from the top surface corresponding to T1, T2, and T3 temperature readings, respectively, to measure axial temperature variations, as shown in Fig. 1. Two additional 4 mm diameter K-type sheathed thermocouples are provided to measure the top and bottom fluid temperature. The mean of two temperature readings is considered the saturated or subcooled temperature of the boiling fluid. A pressure transducer is used to measure the vapour pressure in the chamber. The electrical output from all these sensors is collected and displayed digitally on the panel. Boiling characteristics are observed by a high-speed camera- AOS Promon 501.

2.1.2 Characteristics of Test Surface

A cylindrical test piece of 19mm diameter and 20mm thickness is used for the experiment. All the workpieces are made of copper material and the top surface of the workpiece acts as the test surface. To reduce heat losses from the radial direction and to ensure axial heat conduction in the workpiece, Teflon insulation is provided to the workpiece and heater block assembly, as shown in Fig. 2. The pool boiling experiment is performed on seven different workpieces, which differ in their surface characteristics. Out of these seven workpieces, one workpiece has a plain surface, three workpieces with rectangular finned surfaces, and the rest three have trapezoidal finned surfaces. All these workpieces were fabricated by the computer numerical control (CNC) machining technique. Different parameters of the finned surface, like fin height, fin width, spacing between fins, inclination angle and area enhancement factor, are mentioned in Table 1 and Fig. 3 shows the nomenclature of finned surfaces. The area enhancement factor is the ratio of the actual surface area of the test surface to the projected area of the test surface. The value of the area enhancement factor lies between 1 and 1.891 for different test surfaces. Photographs of three test surfaces are depicted in Fig. 4. The test surface is provided with a particular terminology according to its characteristics; for example, PS refers to a Plain surface, RF refers to a surface with rectangular fins and TF means a trapezoidal finned surface.

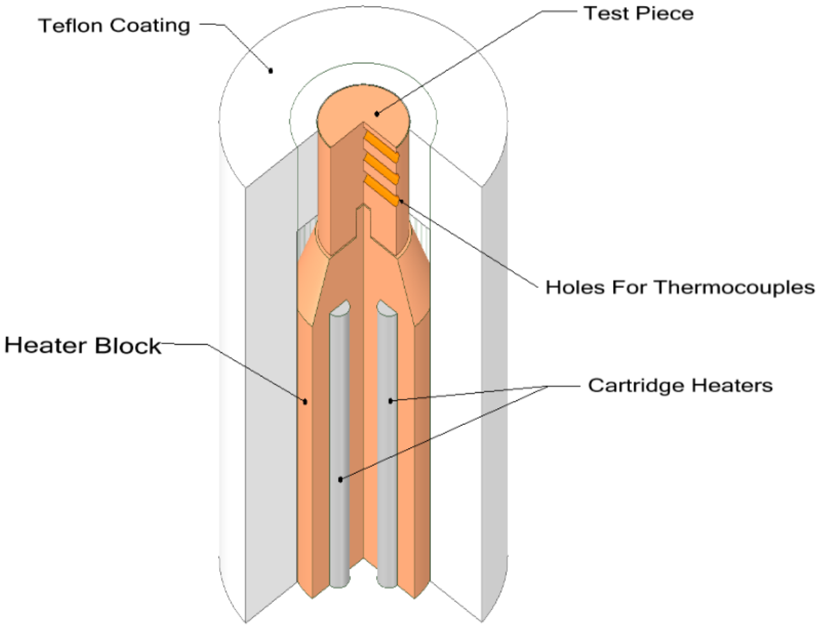

(a)

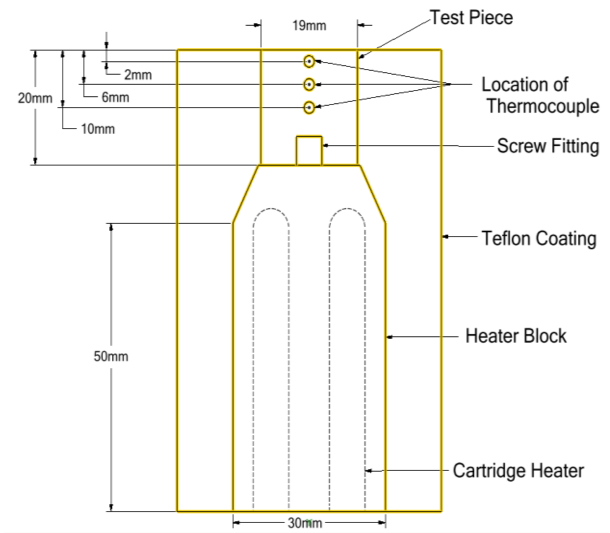

(b)

Fig. 2. Details of the workpiece (a) CAD view, (b) Schematic diagram

Table 1 Characteristic Parameters of Test Surfaces

Test Surface	Fin Height (mm)	Longitudinal Fin Spacing (mm)	Fin width (mm)	Fin Length (mm)	Inclination Angle (deg.)	Area Enhancement Factor
PS	-	-	-	-	-	1
RF1	1	2.14	0.5	1	90	1.391
RF2	1	2.54	0.5	1	90	1.328
RF3	2	2.14	0.5	1	90	1.783
TF1	1	1.6	0.5	1	75	1.431
TF2	1	2	0.5	1	75	1.360
TF3	2	1.6	0.5	1	82.3	1.891

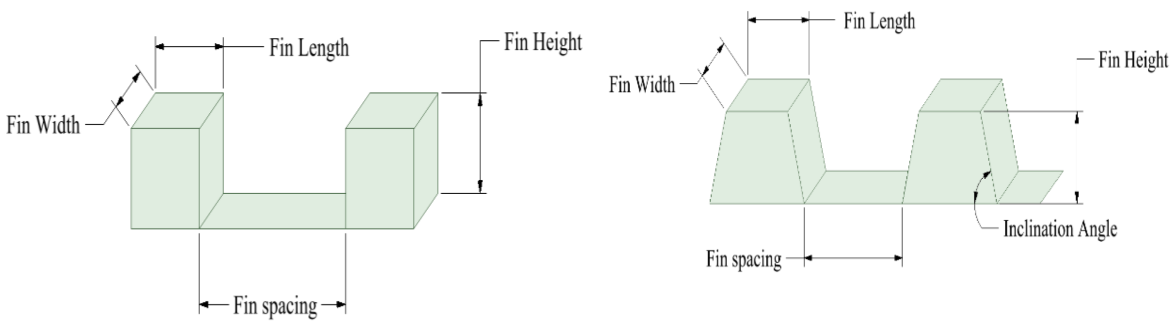

(a) (b)

Fig. 3. Geometric Parameters of fins (a) Rectangular fins, (b) Trapezoidal fins

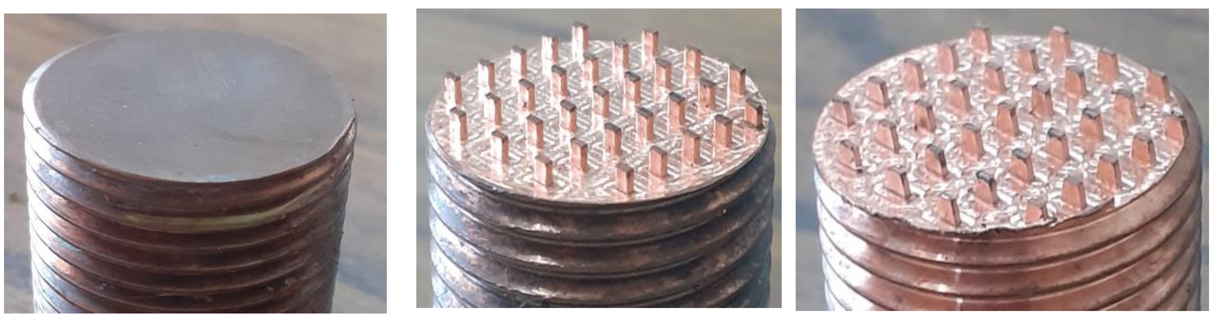

(a) (b) (c)

Fig. 4. Sample Pictures of (a) Plain Test Surface (b) Rectangular Finned Test Surface

(c) Trapezoidal Finned Test Surface

2.1.3 Experimental Procedure

The boiling chamber of the pool boiling apparatus is filled with five litres of distilled water; the same quantity is used for all the experiments. Before starting the experiment, distilled water is boiled vigorously using an auxiliary heater to remove the dissolved gases, known as degassing. During degassing, water should be stirred so that gases accumulated at the corners of the boiling chamber escape easily. After this, the top lid of the boiling chamber is closed, and the water is heated up to 99.9℃ with the help of an auxiliary heater. When the water reaches its saturation temperature, the main heater is switched on and the heat input is given to the workpiece. The steady state for power input is assumed when the change between two consecutive temperature readings is less than 0.2℃. Once the steady state is reached, the power input is increased to a higher value and the experiments are performed up to the permissible power limits of the DC power source. The temperature readings are noted for each power input value, and the same procedure is followed. A closed loop of the cooling water pump, pressure transducer, and PID pressure controller maintains the atmospheric pressure inside the boiling chambers. The PID senses the pressure with the help of a pressure transducer and compares it with the set value and finally sends the signal to the water pump to supply cooling water through the condenser coil. To observe the boiling phenomenon, the light source is switched on at starting of the experiment and a high-speed camera is set at one of the sight glasses available in the boiling chamber.

2.1.4 Data Reduction and Uncertainty Calculation

In the pool boiling experiment, the surface temperature of the workpiece, heat flux, and the HTC between the workpiece and distilled water are calculated. 1-D steady state heat conduction in the axial direction of the workpiece is assumed in the pool boiling experiment. The Fourier law of heat conduction is used to calculate the heat flux value as in Eq. (1).

$$q = -k\frac{dT}{dx} \tag{1}$$

where q is the heat flux between the workpiece and water, *k* denotes the thermal conductivity of copper, whose value is 385 W/(m.K), and dT/dx is the temperature gradient. Taylor's Backward series is used to calculate the temperature gradient from the temperature readings of three thermocouples located 4mm from each other, as in Eq. (2).

$$\frac{dT}{dx} = \frac{3T_1 - 4T_2 + T_3}{2 * \Delta x} \tag{2}$$

where T_1, T_2, and T_3 denote the temperature readings of thermocouples attached at 2mm, 6mm, and 10mm from the top surface of the workpiece. The surface temperature T_s of the workpiece is estimated using Eq. (3).

$$T_s = T_1 - \frac{q * x_1}{k} \tag{3}$$

where x_1 is the distance between the workpiece surface and the top thermocouple. The HTC is calculated by using Eq. (4).

$$h = \frac{q}{T_s - T_{sat}} \tag{4}$$

where $T_{sat.}$ is the saturation temperature of the water.

Some uncertainties are associated with the experiments due to errors in measurements and devices. The propagation of error method is used to estimate the experimental uncertainty in parameters like heat flux, surface temperature and HTC. The uncertainty in the thermal conductivity of copper is 2.33% throughout the operating temperature. Uncertainty in the distance and temperature measurement is ±0.01mm and ±0.1℃, respectively.

To determine the uncertainty in the heat flux, Eq. (5) is used and then dividing these uncertainty values with heat flux values calculated using Eq. (1), the percentage uncertainty in heat flux is obtained. In this work, a maximum uncertainty of 13.07% is observed for the 187.7 kW/m^2 heat flux value of the PS test piece. The uncertainty reduces with the increase in the heat flux, and it becomes 1.904% for a heat flux value of 1300 kW/m^2.

$$U_{q''} = \sqrt{\left[\left(\frac{q''}{k_{Cu}} U_{k_{Cu}}\right)^2 + \left(\frac{3k_{Cu}}{2\Delta x} U_{T_1}\right)^2 + \left(\frac{4k_{Cu}}{2\Delta x} U_{T_2}\right)^2 + \left(\frac{k_{Cu}}{2\Delta x} U_{T_3}\right)^2 + \left(\frac{q''}{2\Delta x} U_{\Delta x}\right)^2\right]} \tag{5}$$

The uncertainty in measuring surface temperature is calculated by using Eq. (6) and a maximum uncertainty of 0.16 ^{0}C is found at the highest heat flux.

$$U_{T_s} = \sqrt{\left[\left(U_{T_1}\right)^2 + \left(\frac{x_1}{k_{Cu}} U_{q''}\right)^2 + \left(\frac{q''}{k_{Cu}} U_{x_1}\right)^2 + \left(\frac{q'' x_1}{k_{Cu}^2} U_{k_{Cu}}\right)^2\right]} \tag{6}$$

The uncertainty in HTC measurement is calculated using Eq. (7) and a maximum of 13.1% uncertainty in HTC is estimated at heat fluxes below 260 kW/m^2 and later, a maximum of 7.4% of uncertainty is estimated for higher heat flux values.

$$U_{HTC} = \sqrt{\left[\left(\frac{U_{q''}}{\left(T_s - T_{sat}\right)}\right)^2 + \left(\frac{q''}{\left(T_s - T_{sat}\right)^2} U_{T_s}\right)^2 + \left(\frac{q''}{\left(T_s - T_{sat}\right)^2} U_{T_{sat}}\right)^2\right]} \tag{7}$$

2.2 Numerical Methodology

A multiphase system is defined as a system that consists of two or more phases. It can be a combination of solid-liquid, liquid-gas, or solid-gas. Nucleate pool boiling falls under the category of liquid-gas multiphase system. In this system, the liquid is treated as a continuous phase and vapour bubbles as a dispersed phase. In this research, we employed the Eulerian multiphase model with Rensselaer Polytechnic Institute (RPI) boiling model for simulating nucleate pool boiling. The Eulerian model is used for modelling discrete and interacting phases in the flow. It is assumed that the volume fraction of every phase is a continuous function of space and time, and the sum of all volume fractions is equal to one. The continuity, momentum, and energy equations are solved for each phase in this model and the same pressure is shared by all phases. Some modifications must be done while applying the equations for a multiphase problem. The changes mainly include the introduction of a volume of fraction, mechanism of mass, momentum, and heat interaction between different phases. ANSYS FLUENT R21.2 commercial software is used to perform a numerical investigation of the pool boiling process.

2.2.1 Heat Flux Partitioning Model -RPI

The heat and mass transfer in nucleate pool boiling is commonly predicted with the help of the RPI wall boiling model. This is a classical wall boiling model that partitioned the total heat flux of boiling into three parts, as shown in Fig. 5 (Kamel et al. (2020)). The convective heat flux is the first part which mainly denotes heat transferred between the test surface and the liquid without any change in the phase. The second part accounts for the latent heat of vaporization absorbed by liquid while changing the phase. The last part is due to the heat transfer between the test surface and the liquid, which fills the space created by the departure of the bubble from the test surface. Equations (8) - (11) show three parts of pool boiling heat flux.

$$\dot{q}_{total} = \dot{q}_{conv} + \dot{q}_{quen} + \dot{q}_{evap} \tag{8}$$

$$\dot{q}_{conv} = h_{conv} A_{conv} \left(T_s - T_l \right) \tag{9}$$

$$\dot{q}_{evap} = V_{bubble} N_a \rho_g h_{lg} \tag{10}$$

$$\dot{q}_{quen} = C_w * \left(\frac{2k_l}{\sqrt{(\pi \alpha_l t_w)}} \right) (T_s - T_l) \, A_{bubble} \tag{11}$$

where $\dot{q_{total}}$ is the total heat flux, $\dot{q_{conv}}$, $\dot{q_{quen}}$, and $\dot{q_{evap}}$ represent the convective, quenching, and evaporative heat flux, respectively. C_w is the bubble waiting time coefficient whose value is by default equal to 1.

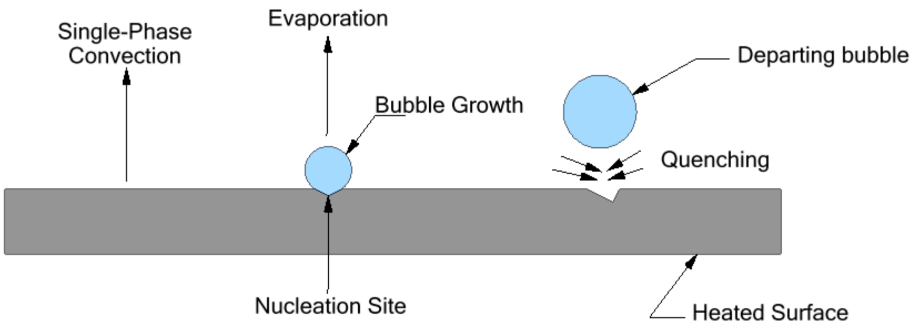

Fig. 5. Heat flux Partitioning Model

2.2.2 Governing equations

Governing equations define a physical problem in terms of mathematical equations. Equations involved in the pool boiling process are the continuity equation, conservation of momentum equation and energy equation given by Eq. (12-14). These equations are solved for two phases present in the process.

$$\frac{\partial(\alpha_k \rho_k)}{\partial t} + \nabla .(\rho_k \alpha_k v_k) = \dot{m}_{kp} - \dot{m}_{pk} \tag{12}$$

$$\frac{\partial\left(\alpha_k \rho_k \vec{v}_k\right)}{\partial t} + \nabla .\left(\rho_k \alpha_k \vec{v}_k \vec{v}_k\right) = -\alpha_k \nabla P + \rho_k \alpha_k \vec{g} + \nabla \tau_k + \left(\dot{m}_{kp} \vec{v}_k - \dot{m}_{pk} \vec{v}_k\right) + S_{1k} \tag{13}$$

$$\frac{\partial(\alpha_k \rho_k E_k)}{\partial t} + \nabla .\left(\rho_k \alpha_k \vec{v}_k E_k\right) = \alpha_k \frac{\partial P}{\partial t} + \nabla \dot{q}_k + Q_{exchange,\, pk} + \left(\dot{m}_{kp} E_k - \dot{m}_{pk} E_p\right) + S_{2k} \tag{14}$$

where subscript k denotes k[th] phase (k = l for liquid and k = g for vapour), and p denotes pressure. ρ_k, α_k , $\vec{v_k}$ are the density, volume fraction and velocity of the k[th] phase, respectively. $\dot{m}_{kp}$ is interfacial mass transfer in the liquid phase on the surface heater. In the momentum equation $\left(\dot{m}_{kp}\overrightarrow{v_k} - \dot{m}_{pk}\overrightarrow{v_k}\right)$ represents the momentum transfer due to liquid evaporation or vapour condensation. Besides, $\left(\dot{m}_{kp}E_k - \dot{m}_{pk}\, E_p\right)$ in the energy equation stands for the energy transfer due to phase change. Additionally, the terms of $\vec{g}$, $\dot{q_k}$, S_{1k}, S_{2k} and $Q_{exchange\,,pk}$ are the gravitational acceleration, heat flux, the inter-phase momentum transfer term, the inter-phase energy transfer term and the direct heat transfer to phase "k".

In the pool boiling process due to the motion of vapour bubbles in the fluid, the boiling process becomes a chaotic phenomenon. We considered a realizable two-equation k-ε model to turbulence. Equations of the k-ε model are mentioned below from Eq. (15 -17)

$$\frac{\partial\left(\alpha_k \rho_k K_k\right)}{\partial t} + \nabla.\left(\rho_k \alpha_k \vec{v}_k K_k\right) = \nabla.\left(\alpha_k \frac{\mu_{T,k}}{\sigma_k}\right) + \alpha_k \tau_{T,k} \nabla v_k - \alpha_k \rho_k \varepsilon_k + S^{int}_{k,k} \tag{15}$$

$$\frac{\partial\left(\alpha_k \rho_k \varepsilon_k\right)}{\partial t} + \nabla.\left(\rho_k \alpha_k \vec{v}_k \varepsilon_k\right) = \nabla.\left(\alpha_k \frac{\mu_{T,k}}{\sigma_k}\right) + \alpha_k \frac{\varepsilon_k}{K_k}\left(C_{\varepsilon 1} \tau_{T,k} v_k - C_{\varepsilon 2} \rho_k \varepsilon_k\right) + S^{int}_{\varepsilon,k} \tag{16}$$

$$\tau_{T,k} = \mu_{T,k}\left[\nabla \vec{v}_k + \left(\nabla \vec{v}_k\right) - \frac{2}{3}\left(\nabla . \vec{v}_k\right) \mathrm{I}\right] - \frac{2}{3} \rho_k K_k \mathrm{I} \tag{17}$$

Here k and ε are denoted as turbulent kinetic energy and dissipation rate. $\mu_{T,k}$ is the turbulent viscosity coefficient, $S^{int}_{k,k}$, $S^{int}_{\epsilon,k}$ are the source terms related to the interaction of nucleate bubbles with the turbulent flow of the liquid.

2.2.3 Model Closure for the RPI Wall Boiling Model

The interaction between different phases induces forces like drag force, lift force, wall lubrication force, turbulent dispersion force, etc. All these forces are included in the momentum equation as part of the source term (S_{1k}) written on the right side of the equation (13). The information regarding these forces is mentioned below (ANSYS Fluent Theory Guide)

2.2.3.1 Drag force

In the commercial software ANSYS FLUENT, several models are available for drag coefficient like Ishii, Schiller Neumann, Grace and Tomiyama, etc. Out of these models, Schiller Neumann is suitable for almost all types of flows. But in this simulation, we used the Ishii darg model, which can be applied for boiling flow problems. Expression for the model is given in equation (18)

$$C_D = \min\left(C_D^{vis},\, C_D^{dis}\right) \tag{18}$$

Where C_D is the drag coefficient and is equal to the minimum viscous drag or distorted drag coefficient. Equations used to calculate viscous drag (C_D^{vis}) and distorted drag (C_D^{dis}) coefficients are given in Eq. (19) and Eq. (20).

$$C_D^{vis} = \frac{24}{Re} * \left(1 + 0.15Re^{0.75} \right) \tag{19}$$

$$C_D^{dis} = \frac{2}{3} * \frac{d_{bubble}}{\sqrt{\frac{\sigma}{g\left(\rho_l - \rho_g \right)}}} \tag{20}$$

where Re is the relative Reynold number of vapour phase, σ denotes the surface tension, g is the acceleration due to gravity and d_{bubble} represents bubble departure diameter. ρ_l and ρ_g are liquid and gas phase densities, respectively. The Relative Reynold number can be calculated using Eq. (21)

$$Re = \frac{\rho_{vapor} \left(v_{vapor} - v_{liquid} \right) d_{bubble}}{\mu_{vapor}} \tag{21}$$

2.2.3.2 Lift force

The lift force in the multiphase flows mainly acts due to the velocity gradient in the primary phase flow. The magnitude of lift force depends on the diameter of the particles. This force can be neglected if the diameter of a particle is small. In the present simulation, we selected the Tomiyama model to include lift force. Tomiyama model is applicable for large-scale deformable bubbles of ellipsoidal and spherical regimes.

2.2.3.3 Wall lubrication force

Wall lubrication force tends to push the secondary phase away from the walls. The model of Antal et al. is used to calculate the coefficient of wall lubrication. This model applies to very fine mesh. Expressions for wall lubrication force and the coefficient is shown below in Eq. (22) and (23).

$$F_{k,LW} = C_{WL} \rho_l \alpha_g \left| \vec{v}_l - \vec{v}_g \right|^2 \vec{n}_w \tag{22}$$

$$C_{WL} = \max\left(0, \frac{C_{W1}}{d_{bubble}} + \frac{C_{W2}}{y_W}\right) \tag{23}$$

where $F_{k,LW}$ is wall lubrication force, C_{WL} is wall lubrication coefficient. $\overrightarrow{n_w}$ is the unit normal pointed away from the wall, ρ_l is the density of the pure liquid and y_W is the distance to the nearest wall. C_{W1} = -0.01 and C_{W2} = 0.05 are non – dimensional coefficients, respectively.

2.2.3.4 Turbulence dispersion force

This force accounts for turbulent momentum transfer between the interphases. The Lopez de Bertodano model is used to include this force. Turbulent dispersion force acts as turbulent diffusion force in dispersed flow. Eq. (24) gives the expression for turbulence dispersion force.

$$F_{l,\ dispersion} = -F_{g,\ dispersion} = C_{TD}\,\rho_l\,K_l\,\nabla\alpha_g \tag{24}$$

Where C_{TD} – a user-defined constant, by default, equal to 1. K_l is the turbulent kinetic energy in the liquid phase. $\nabla\alpha_g$ is the gradient of the vapour phase volume fraction.

2.2.3.5 Interfacial Mass and Heat Transfer

In this case, we considered the phase change of water from liquid to vapour and to specify this mass transfer, we selected the Boiling model. The boiling model takes care of all the boiling parameters like nucleation site density, bubble departure diameter, bubble departure frequency and area of influence. For all these parameters, we used default settings, i.e., Cole model for bubble departure frequency, Lammert and Chawla for active nucleation site density and bubble departure diameter, and Tolubinski and Kostanchuk and Del Valle and Kennings for the area of influence. Equations related to these models are given below from Eq. (25)-(27).

Cole correlation equation

$$f = \left(\frac{4\,g\left(\rho_l - \rho_g\right)}{3\,\rho_l\,d_{bubble}}\right)^{\frac{1}{2}} \tag{25}$$

where f denotes the frequency of departure, g – acceleration due to gravity, d_{bubble} - bubble departure diameter, ρ_l & ρ_g are liquid and vapour density.

Lammert Chawla equation

$$N_a = C^n\left(T_w - T_{sat}\right)^n \tag{26}$$

Where N_a – active nucleation site density, C and n are constants, T_w & T_{sat} are the temperature of the wall and saturation temperature of the liquid.

Tolubinski and Kostanchuk correlation

$$d_{bubble} = \min\left(0.0014,\ 0.0006\,e^{\frac{T_w - T_{sat}}{45.0}}\right) \tag{27}$$

Where d_{bubble} denotes departure diameter, T_w & T_{sat} are the temperature of the wall and saturation temperature of the liquid. This correlation is the default for the RPI model.

Heat transfer between the continuous phase (water) and the dispersed phase (vapour) in the boiling process is included in the simulation. This can happen in pool boiling due to non-thermal equilibrium across the interphase. To account for heat transfer, Ranz–Marshall model is selected. It gives a correlation for the heat transfer coefficient as represented by expressions (28) and (29).

$$Nu_g = 2.0 + 0.6\, Pr_l^{0.333}\, Re_g^{0.5} \tag{28}$$

$$h_{gl} = \frac{k_l\, Nu_g}{d_{bubble}} \tag{29}$$

where Nu_g is Nusselt number of dispersed phases, Pr_l is Prandtl number of continuous phases, Re_g is Reynold number of vapour phase depends on bubble departure diameter and relative velocity, h_{gl} denotes heat transfer coefficient, d_{bubble} is bubble departure diameter. k_l denotes the thermal conductivity of the liquid.

2.2.4 Computational Geometry

In the present work, a 2-D rectangular boiling chamber is considered. The computational geometry is like that of the experimental boiling chamber and three types of geometry are used. The first geometry consists of a boiling chamber with a plain test surface, while the second geometry has a rectangular finned test surface and finally, the third one contains a heater with trapezoidal fins on the surface. All the test surfaces are 19mm in diameter, made up of copper material and placed in the horizontal direction at the bottom of the boiling chamber. The length and height of the chamber are 250mm and 150mm, respectively. Figure 6 illustrates the structure of the geometries used in the simulations. The top side is open to the atmosphere, the side walls are assumed to be adiabatic, and the test surface is placed at the centre of the 2-D boiling chamber.

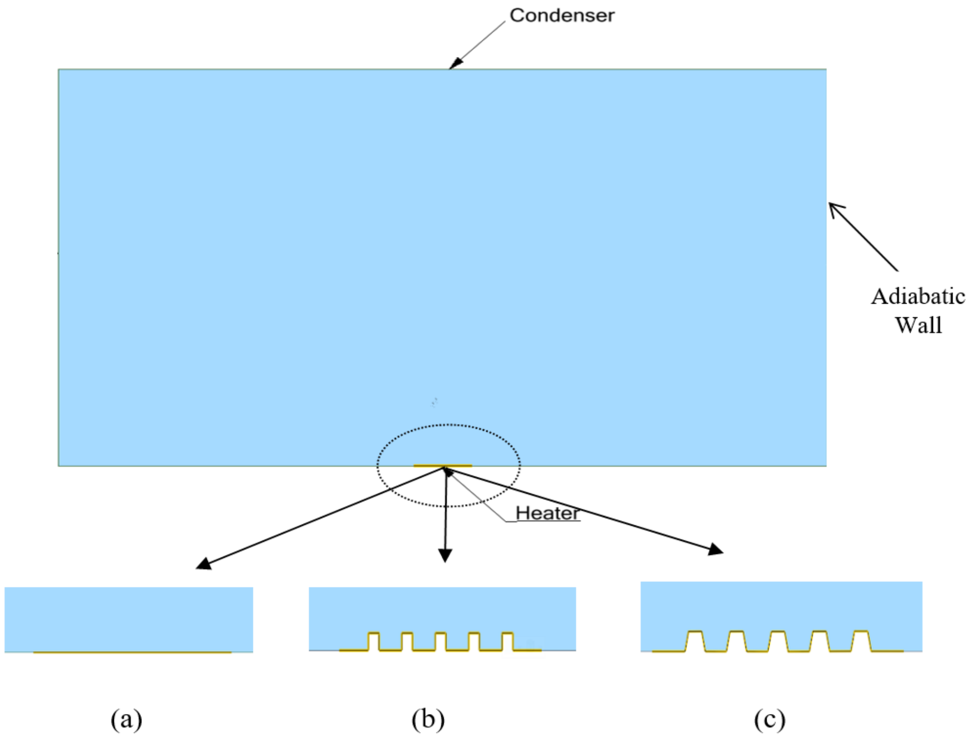

Fig. 6. Computational geometry of Present Numerical Study (a) Plain Test Surface (b) Rectangular Finned Test Surface (c) Trapezoidal Finned Surface

2.2.5 Meshing

The computational grid is generated using ICEM CFD software. The accuracy of numerical results directly depends on the quality of meshing and the quality can be determined by some parameters like skewness, orthogonality, aspect ratio, smoothness, etc. The structured grid usually provides better mesh quality and reduces the number of computational cells, thus reducing the computational time. Due to these reasons, we used a structured grid for the meshing of computational geometry. In the case of finned test surface geometry, the fine meshing of element size 0.5mm is used near the finned surface in both x and y directions and coarser mesh at a farther distance from the fins. But denser mesh at one location can lead to data accumulation at that area, resulting in divergence and inaccurate results. So, non–uniform meshing should be done carefully and the transition between fine and coarse mesh should be smooth. Figure 7 shows the computational domain with a structured grid.

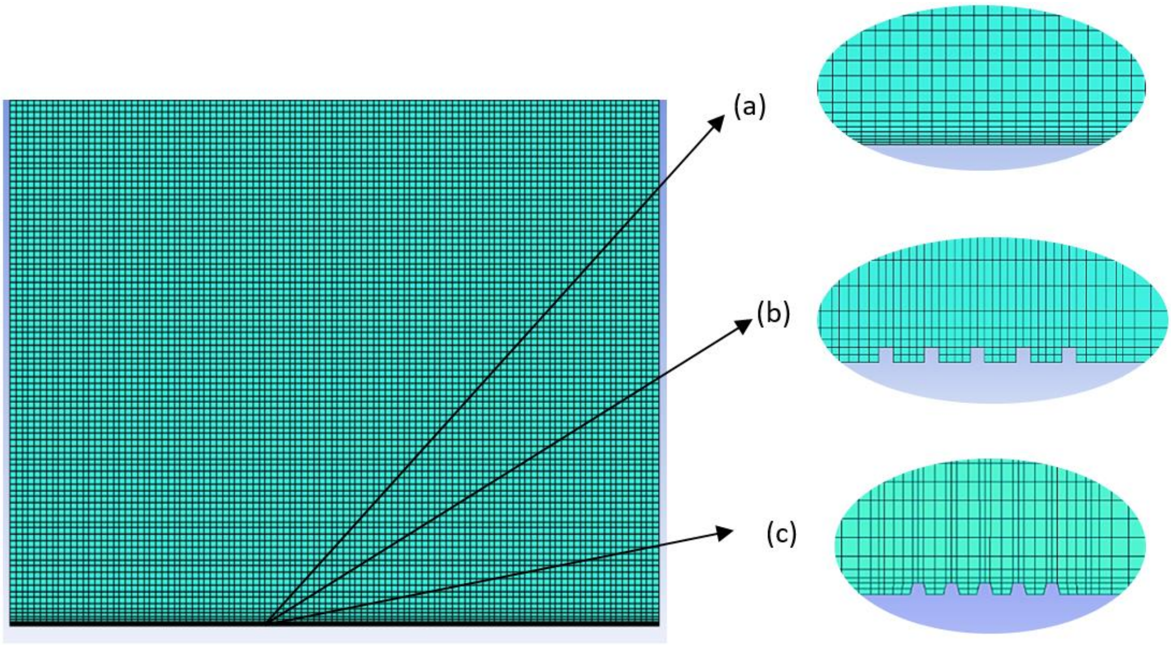

Fig. 7. Computational Grid of the Boiling chamber with (a) Plain Test Surface (b) Rectangular Finned Test Surface (c) Trapezoidal Finned Test Surface

2.2.6 Boundary conditions and Initial conditions

In this simulation, the governing equations are subjected to the following boundary conditions. The test surface is maintained at a constant wall temperature as mentioned in Kamel et al. (2020), Feroskhan et al. (2022), and Enjadat et al. (2022), $T = T_w$ which is the quasi-steady state temperature measured in the experimental setup.

All side walls and bottom surfaces except the test surface are at the adiabatic condition which means heat flux will be zero.

$$\acute{q} = -k_w \frac{dT}{dx} = 0 \tag{30}$$

The top surface of the boiling chamber is assumed to be at atmospheric pressure, $P = P_{atm}$

Initial conditions in the computational model were identical to the experimental test case i.e., the bulk mean temperature of liquid water is assumed as the saturation temperature (373.15 K.) at 1 atmospheric pressure. As the simulation proceeds, the liquid in the vicinity of the test surface becomes superheated due to heat exchange from the test surface. Moreover, the initial velocity of water is kept at zero. The temperature of vapour bubbles is also assumed to be fixed at 373.15K. Table 2 presents the properties of liquid water and water vapour at the saturation temperature of 373.15 K (Alimoradi et al. (2022) and Zhang et al. (2019)).

Table 2 Thermophysical Properties of Phases at 373.15K

Properties	Water liquid	Water vapour
Density (kg/m^3)	958.35	0.59817
Specific heat (J/Kg K)	4215.7	2080
Thermal conductivity (W/m K)	0.67909	0.02509
Dynamic viscosity (Pa-s)	0.000281	0.0000122
Surface tension (N/m)	0.0589	-

2.2.7 Solution Procedure

A finite volume-based solver ANSYS FLUENT is used to solve the governing equations within specified initial and boundary conditions. A phase-coupled SIMPLE method (PC-SIMPLE) is used to handle the pressure-velocity coupling. In this algorithm, the velocities are solved coupled by phases in a segregated manner, whereas the pressure correction equation is built based on the total continuity. A second-order upwind scheme is used to approximate the momentum, turbulent kinetic energy and turbulent dissipation rate, and the gradient of all flow variables are calculated using the least-square cell-based method. Moreover, to solve the vapour volume fraction equation in a multiphase flow solver, the upwind scheme is generally undesirable for interface tracking because of the overly diffusive nature which results in the unphysical thickening of the fluid interfaces. Hence, to take advantage of the stability of upwind differencing and the accuracy of down winding for interface tracking, a modified scheme i.e., High-Resolution Interface-Capturing (HRIC) scheme is used for the current simulations. Hence, the following assumptions are considered during the present simulation-

- The simulations are transient, and turbulence is modelled in them.
- The thermophysical properties of both phases are assumed to be constant.

2 RESULTS & DISCUSSION

3.1 Experimental Results

3.1.1 Validation of Experimental Result

To examine the reliability of experimental data, the results are compared with that of published experimental results of Inoue et al. (2002) carried out under similar experimental conditions. In addition to this, results were also compared with Cooper (1984), Gorenflo (1997) and Nishikawa-Fujita (1982) correlations. Figure 8 shows the HTC versus heat flux curve for the present results. Any deviation of experimental results from correlations can be attributed to factors like differences in test surface characteristics, geometry and size of the boiling surface, experimental conditions etc. used to derive the correlations. It can be seen from Fig. 8 that the present result follows a trend that is similar to that predicted from Cooper's (1994) correlation. The mean absolute error (MAE) between the predicted results of Gorenflo (1997), Cooper (1994), and Nishikawa-Fujita (1982) and the present experimental results comes out to be 17.6%, 15.4% and 15.5% respectively. The mean absolute error can be determined by using Eq. (31)

$$MAE = \frac{1}{i} \sum \frac{\left| q_{exp.} - q_{pred.} \right|}{q_{exp.}} X\, 100 \qquad (31)$$

Apart from this, at the lower heat flux values (less than 200 kW/m^2), the HTC of present results is slightly higher than the HTC values of Inoue et al. (2002). At a lower value of HTC, the uncertainty in the result is high, approximately 13.17% and the uncertainty decreases as the HTC value increases. Inoue et al, (2002) observed a change in the slope of the boiling curve and the boiling curve was divided into two regions: high heat flux (HHFR) and second transient region (STR). We did not observe such a difference. This signifies that the present experimental result is consistent with the previously published literature.

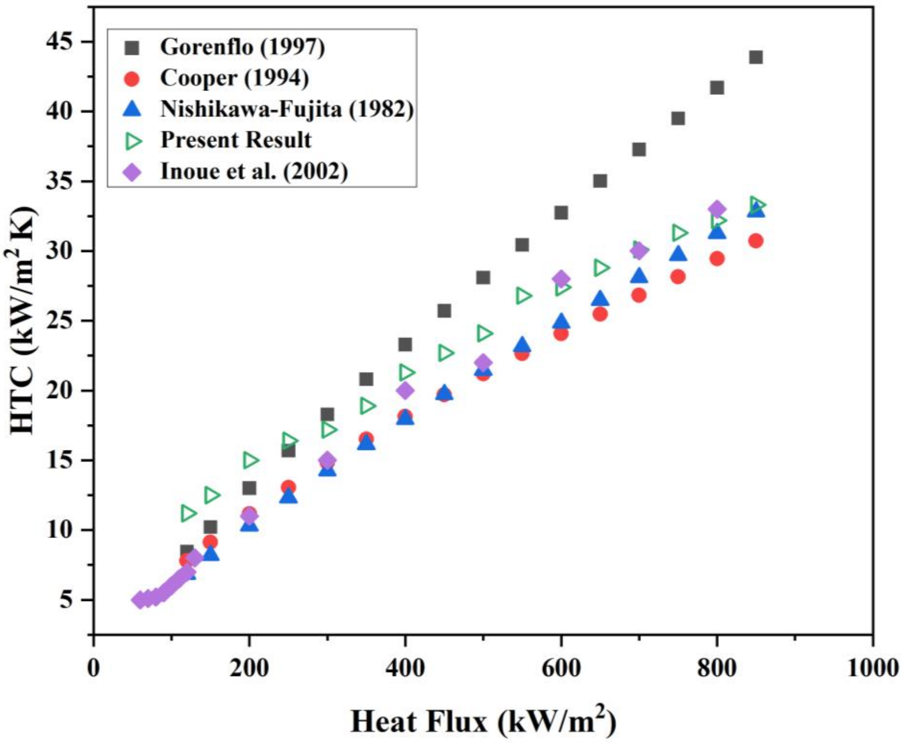

Fig. 8. Validation of Experimental Result

Experimental results of the pool boiling process are also examined for the repeatability test. To check the repeatability of results, three test runs are conducted for the PS test piece whose boiling curves are shown in Fig. 9. The results indicate that the boiling curves for all three tests are in good agreement with each other. This clearly shows that the results obtained through the present experimental studies are reliable.

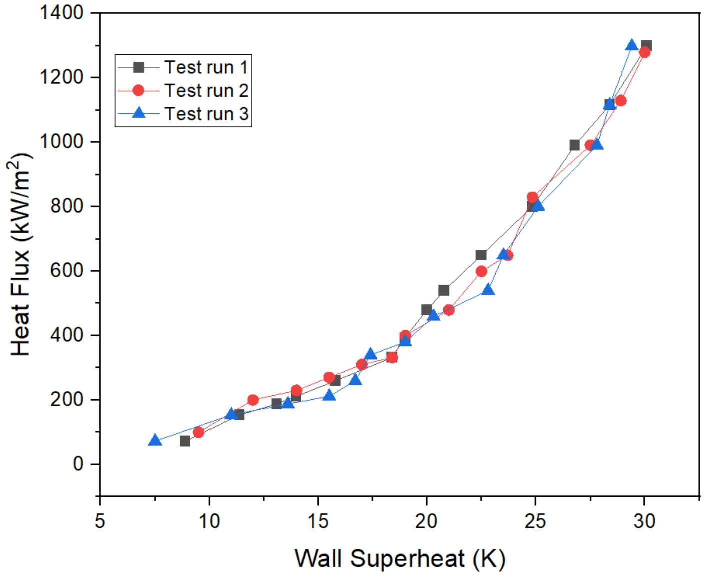

Fig. 9. Repeatability test of three runs of Pool boiling experiments

3.1.2 Effect of Fin geometry on boiling heat transfer

The influence of adding fins on the surface and fin geometry is depicted in Figure 10. The measurement uncertainties are shown in error bars in the figures. The variation of wall heat flux with the wall superheat, which is also known as the pool boiling curve, is presented in Fig. 10 (a) for the plain surface (PS), rectangular fins (RF) and trapezoidal fins (TF). A monotonous increment in the heat flux is noticed for all the investigated surfaces, with the increment in the wall superheat within the range studied. However, the rate of increment in the heat flux value differs for different surfaces investigated in this study. It can be observed from this figure that the boiling curves of finned surfaces have a leftward shift as compared to the plain surface, which indicates an improvement in heat flux for the same wall superheat value. For example, there is an improvement of 52.3% and 101.5% in the heat transfer performance of RF1 and TF1 respectively as compared to the plain test surface at 20K wall superheat. Similarly, a significant improvement in the HTC can be observed from Fig. 10 (b). A minimum increment of 11.09% is observed for a value of heat flux = 1300 $\frac{kW}{m^2}$ for RF1 and an increment of 26.19% for a value of heat flux = 1300 $\frac{kW}{m^2}$ for TF1. A maximum increment of 37.3% is observed for a value of heat flux = 275 $\frac{kW}{m^2}$ for RF1 and an increment of 119.2% for heat flux = 178 $\frac{kW}{m^2}$ for TF1.

The increment in the heat flux value/ HTC value is because of the increased surface area for the finned surfaces compared to the plain surface. The additional surface area promotes the number of active nucleation sites on the test surface and enhances boiling heat transfer. Moreover, the increment in the heat flux value or HTC value for TF1 over RF1 can be attributed to the shape of the fin. For TF1, the bubbles can easily move upward due to the wider space available at the fin tip without much restriction from the side walls of fins after nucleating at the fin root. In contrast, in rectangular fins, the width remains the same from the top to bottom and the bubble movement is somewhat restricted.

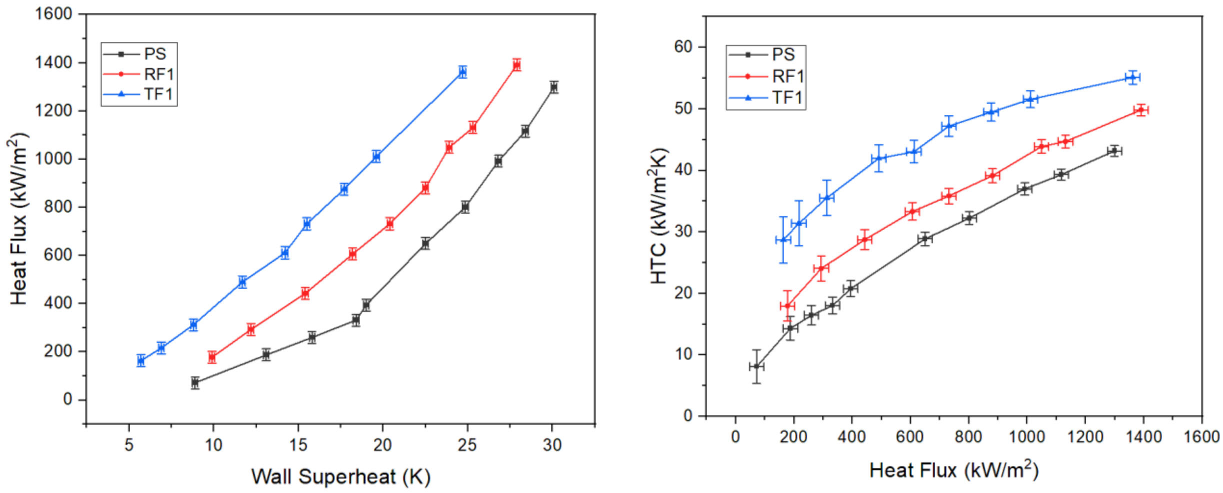

(a) (b)

Fig. 10. Boiling curves for PS, RF1, TF1 (a) Heat flux v/s wall superheat (b) HTC v/s heat flux

In the pool boiling process, discrete vapour bubbles of smaller diameter initially nucleate at some locations. But after some time, with the small increase in wall superheat, there is an increase in the number of active nucleation sites and bubble size. Bubbles coalesce, and boiling becomes vigorous with the larger bubble departure diameter on further increase in the wall superheat. Apart from this, we observed that at lower heat flux values in finned surfaces, bubbles first nucleated at the fin root because the temperature of the fin root is higher as compared to the fin tip. As the heat flux value increases, the bubbles randomly start nucleating at the fin tip and fin root. Figure 11 shows the nucleation of bubbles on different test surfaces, whereas Fig. 12 indicates the bubble growth and departure of bubble nucleated at the fin root of test surface TF1. The bubbles at the fin tip depart faster than those at the fin root because of less surface tension force at the fin tip. These additional vapour bubbles contributed to the heat flux.

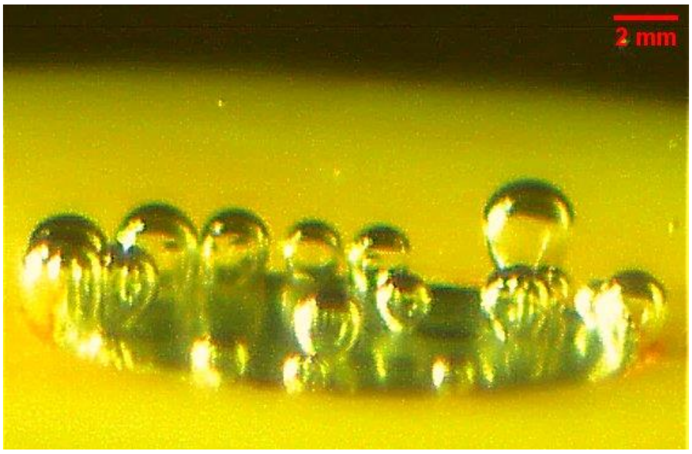

(a)

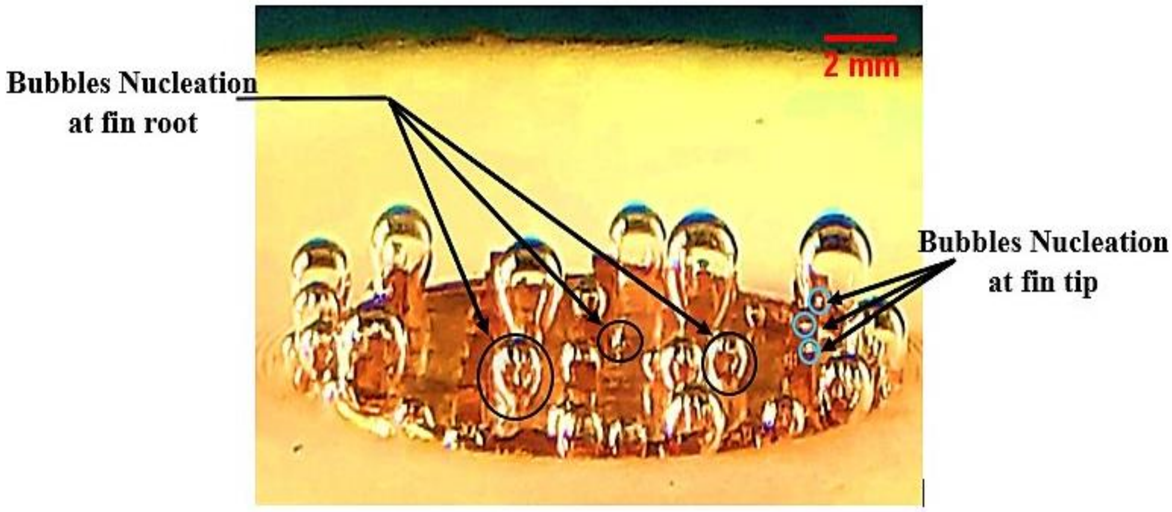

(b)

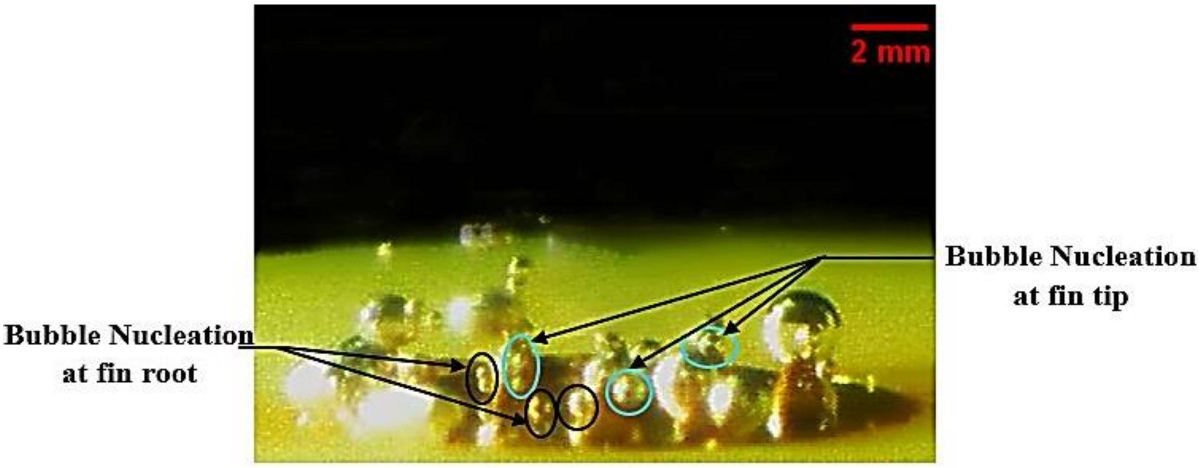

(c)

Fig. 11. Bubble nucleation for (a) Plain test surface, (b) Rectangular finned test surface, (c) Trapezoidal finned test surface

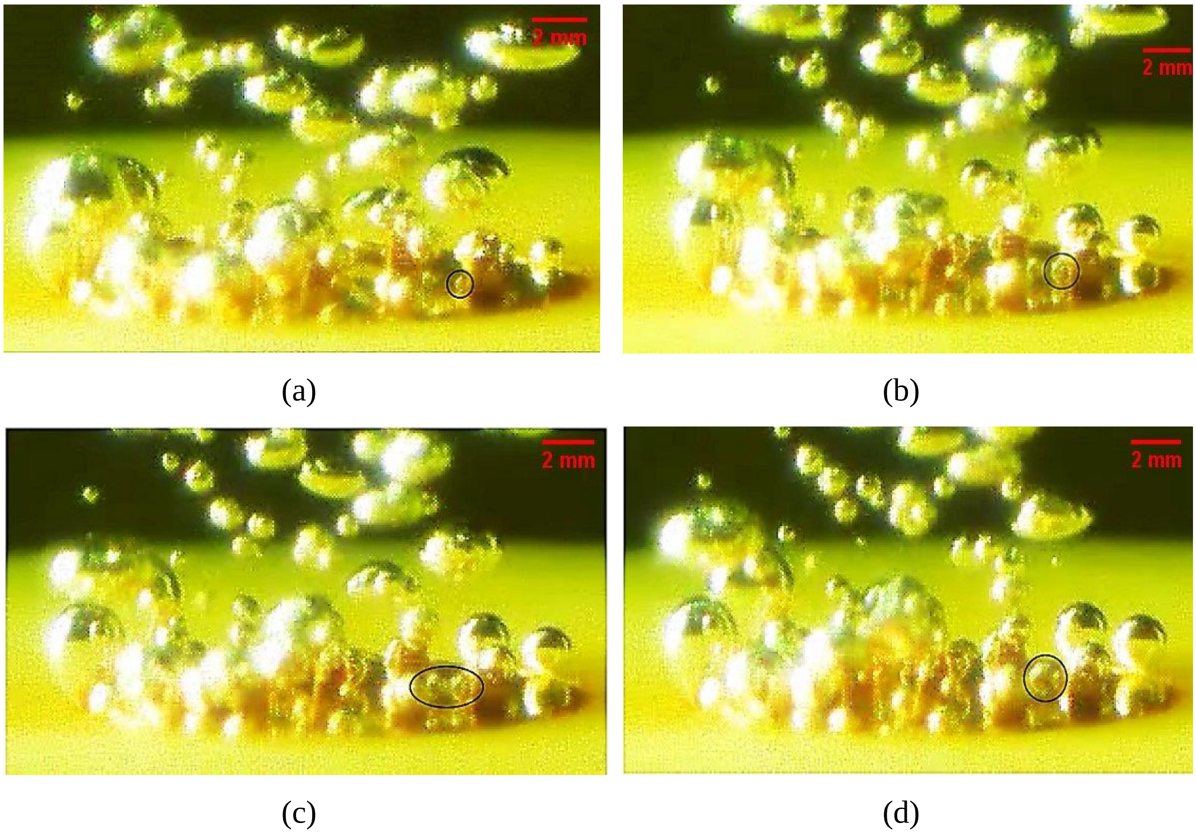

Fig. 12. Bubble growth at fin root of TF1 test surface (a) Nucleation of bubble (t =0 ms), (b) Bubble growth (t =6 ms), (c) Bubble Coalescence (t =8 ms), (d) Bubble departure (t =13 ms)

3.1.3 Effect of Fin Parameters on Boiling heat transfer

Experiments are carried out to understand the effect of fin spacing on the pool boiling heat transfer. Figure 13 shows the pool boiling performance of finned surfaces with different fin spacing and their heat flux values are compared with the plain surface within a certain range of wall superheat. Results illustrate that the increase in the fin spacing has adversely affected the pool boiling heat transfer from both finned surfaces RF and TF. The test surface RF1 has performed better than the RF2 surface and a similar trend is observed for test surfaces TF1 and TF2. To exemplify, at the wall superheat of 15K, there is a 27% and 18% reduction in heat flux value for RF2 and TF2 compared to the surfaces RF1 and TF1, respectively. The heat transfer rate in the pool boiling process is proportional to the bubble departure frequency from the heated surface. Because the volume of a merged bubble is slightly larger than the sum of the volumes of two separate bubbles before the merger, the buoyant force acting on the bubble ultimately increases, promoting the rate of bubble departure. This helps lift the bubble from the heated surface. The faster bubble departure paves the way for the nucleation of new bubbles. Figure 14 depicts the boiling flow patterns on different test surfaces. The figure shows that a row of smaller diameter bubbles nucleated at the fin root of RF2 and TF2. The bubble departure diameter is 1.75mm and 1.15mm for the surfaces RF1 and RF2, respectively, at the heat flux of 180 kW/m^2. Similarly, at 150 kW/m^2 heat flux, the bubble departure diameters from TF1 and TF2 surfaces are 2.08mm and 1.8mm. The large fin spacing restricts the bubble interaction and merging, which is responsible for a smaller bubble departure diameter in the case of test surface TF2 compared to test surface TF1. In test surface TF1, the possibility of bubble merger (lateral direction) is more due to small spacing, resulting in higher heat flux values. Apart from this, with the increase in fin spacing, the thermocapillary action of surrounding liquid also decreases, reducing the rewetting of the dry-out surface produced after the bubble departure and ultimately affecting the quenching heat transfer. Jiang et al. (2021) also reported that smaller fin spacing results in higher heat flux for the same wall temperature and they attributed this to the enhanced thermocapillary forces inducing quick rewetting at smaller fin spacing. On comparing the boiling curve of the surface RF1 and TF2, we found that despite having approximately similar fin spacing of these test surfaces, surface TF2 had improvement over RF1.

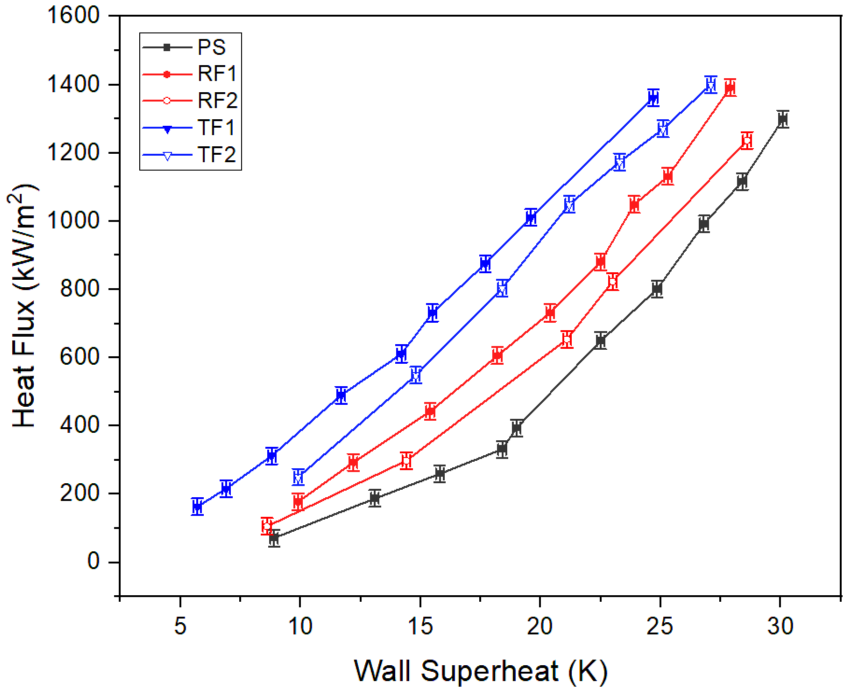

Fig. 13. Effect of fin spacing on boiling heat transfer

(RF1 spacing = 2.14mm, RF2 spacing = 2.54mm, TF1 spacing= 1.6mm, TF2 spacing= 2mm)

This result indicated that apart from the vapour bubbles, the convection heat transfer between the test surface and liquid also plays an important role in heat transfer from the trapezoidal finned surface. Moreover, the inclined shape of trapezoidal fins provides a better liquid supply to the test surface. So, increasing fin spacing reduces the pool boiling performance, but still, the performance of the surfaces RF2 and TF2 is better than the plain test surface.

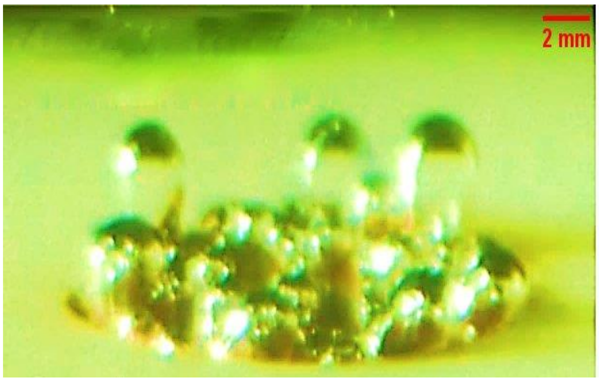

Vapour Bubbles on RF1 at 180 kW/m^2

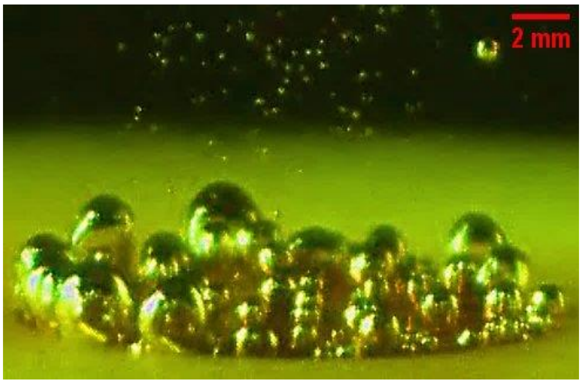

Vapour Bubbles on RF2 at 180 kW/m^2

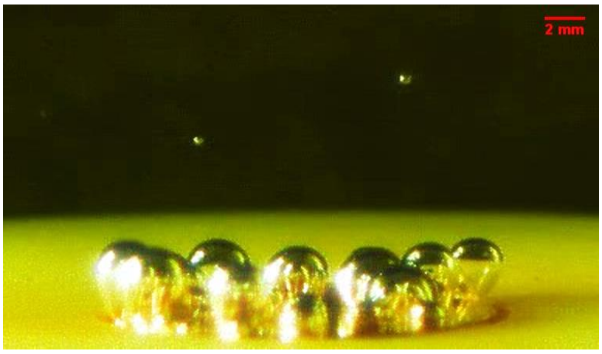

Vapour Bubbles on TF1 at 150 kW/m^2

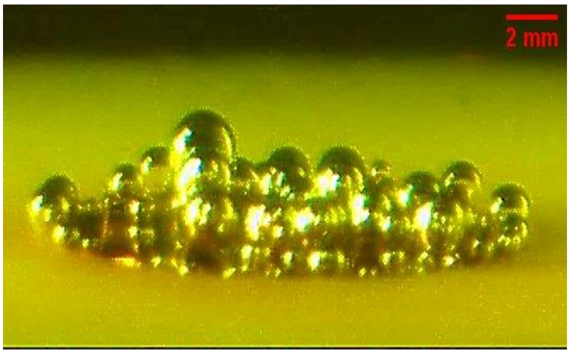

Vapour Bubbles on TF2 at 150 kW/m^2

Fig. 14. Boiling flow patterns on different test surfaces

The impact of fin height on the pool boiling performance of test surfaces is highlighted in Fig. 15. It is observed that the larger fin height is beneficial for enhancing the boiling heat transfer from the test surfaces. The boiling curve of RF3 and TF3 has reported a leftward shift from that of RF1 and TF1 surfaces, which indicates improvement in the boiling heat transfer performance of RF3 and TF3 surfaces. With the increase in fin height, there is an improvement of 64% and 9.3% in heat flux dissipated from RF3 and TF3 compared to RF1 and TF1. Similar results were presented by Jiang et al. (2021), who observed increased heat flux with the increase in height of the cylindrical pillars and Nirgude and Sahu (2017), who observed increased heat flux with the increase in depth of the tunnel geometries. Increasing the height of the fins encourages the merging of bubbles as it results in a greater surface area. This, in turn, leads to a stronger surface tension force acting on the departing bubbles. The surface tension hinders the bubble from detaching, compelling them to grow within the available space between the fins. As a result, the bubbles attempt to merge with nearby bubbles, increasing their size. This enlargement of bubble diameter enhances the buoyancy force acting on the bubbles, thereby promoting their departure from the heated surfaces.

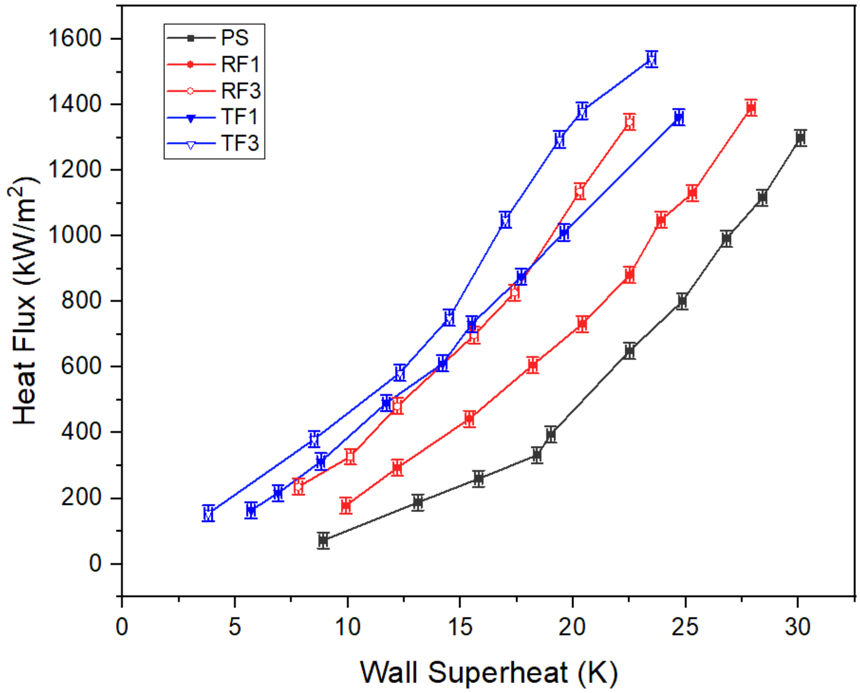

Fig. 15. Effect of fin height on boiling heat transfer

(RF1 ht.=1mm, RF3 ht.= 2mm, TF1 ht.=1mm, TF3 ht. = 2mm)

Figures 16 and 17 show vapour bubbles nucleating at the different test surfaces. For the test surfaces RF1 and RF3, the bubble departure diameter is 1.98mm and 2.2mm, respectively, at 300 kW/m^2 heat flux. This implies that the merging of the bubbles is not significant here, but the RF3 test surface has a greater area enhancement factor (1.783) which results in the nucleation of more bubbles on the test surface.

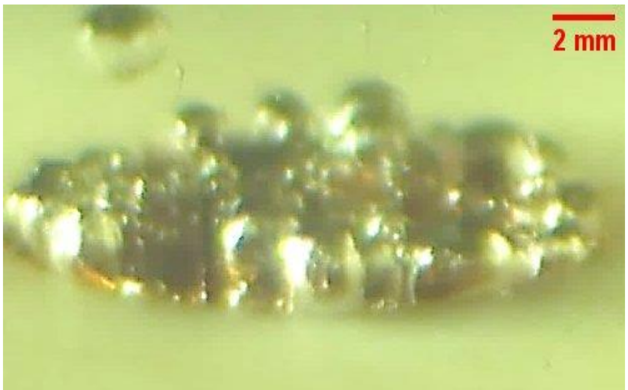

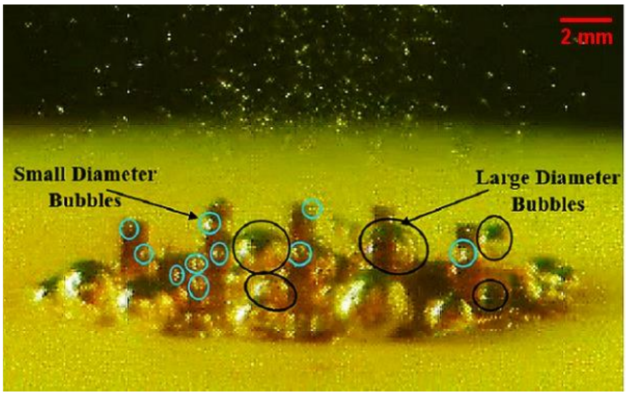

(a) (b)

Fig. 16. Bubble visualization on test surfaces (a) RF1 (b) RF3 at a heat flux of 300 kW/m^2

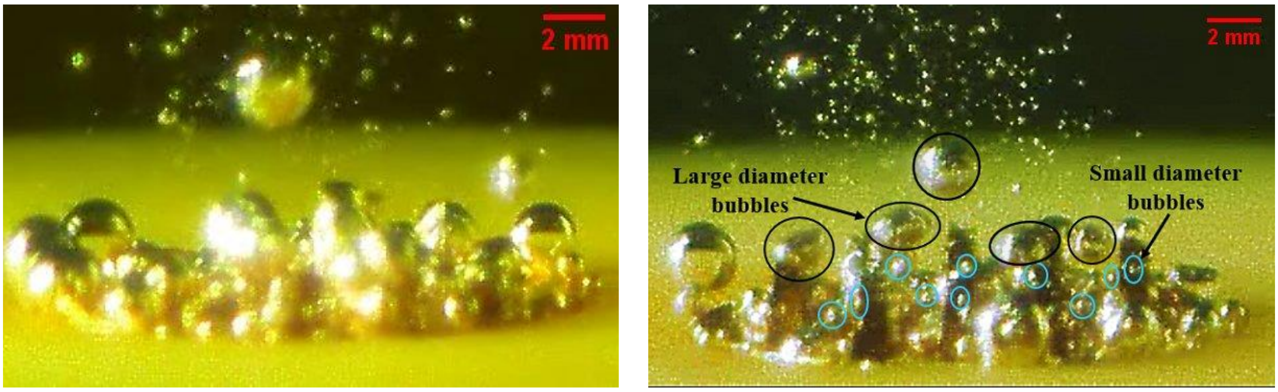

(a) (b)

Fig. 17. Bubble visualization on test surfaces (a) TF1 (b) TF3 at a heat flux of 300 kW/m^2

From these figures, we can see that the fins of the RF1 surface are entirely covered by bubbles from the test surfaces, which reduces the surface area available for further heat transfer. But for the RF3 surface, we can observe that some tiny bubbles nucleate from the fin tip and larger diameter bubbles from the space between the fins. This mainly contributes towards 64% heat flux enhancement in the RF3 surface. In the trapezoidal finned surfaces, the angle of inclination of fins changes with the change in the finned structure height. The inclination angle is 82.3º and 75º for test surfaces TF3 and TF1, respectively. This increase in the inclination angle reduces the benefit of the trapezoidal-shaped fins because the bubble dynamics, in this case, may closely follow that of the rectangular fins with an inclination angle of 90º. There is a slight improvement in TF3 because trapezoidal fins promote the formation of larger bubbles in the lateral direction due to their shape. The bubble departure diameters for TF1 and TF3 are 2.53mm and 2.68mm.

Figures 18 and 19 show the variation of HTC corresponding to the heat flux for different fin parameters. Results demonstrated that the HTC depends on the area available for pool boiling heat transfer. From the figures, we observed that the HTC is directly proportional to the surface area of the test surface. Figure 18 shows that the test surface TF2 has the lowest HTC values compared to RF1, TF1 and TF2. This mainly happens because the TF2 has the largest fin spacing of 2.54 mm, reducing the number of fins on the test surface. The lower value of the area enhancement factor (1.328) results in reduced HTC of TF2 in both lower and higher heat flux regions. At lower wall superheat, a major part of the heat is transferred due to convection between solid test surface and fluid. With the increase in fin spacing, the number of fins on the test surface reduces, which results in a decrease in convection heat transfer. It is evident from Fig. 18 that maximum reduction in HTC is observed at low heat flux values, which are 15.8%

for RF2 for a heat flux of 180 $\frac{kW}{m^2}$ and 22.6% for TF2 for a heat flux value of 250 $\frac{kW}{m^2}$when compared with HTC of RF1 and TF1. But at higher heat flux values, decrement in HTC is less because at higher heat flux values, heat transfer occurs due to the nucleate boiling phenomenon. Figure 19 demonstrates the variation of HTC with respect to heat flux values for the test surfaces with different fin heights. The results indicate an improvement in HTC as the height of fins increases. The possible reason is the enhancement in convection heat transfer due to additional area provided by higher fins. Moreover, it can be seen from the curve that as we move from lower heat flux to higher heat flux values, the slope of the HTC curve keeps on decreasing. One reason may be the change in the area available for the nucleation of bubbles. At lower heat fluxes, there are distinct bubbles of tiny size, and as a result, there is enough area for additional nucleation sites. But at higher heat flux values the test surface is completely covered with bubbles of larger diameter and there is no space left for further nucleation.

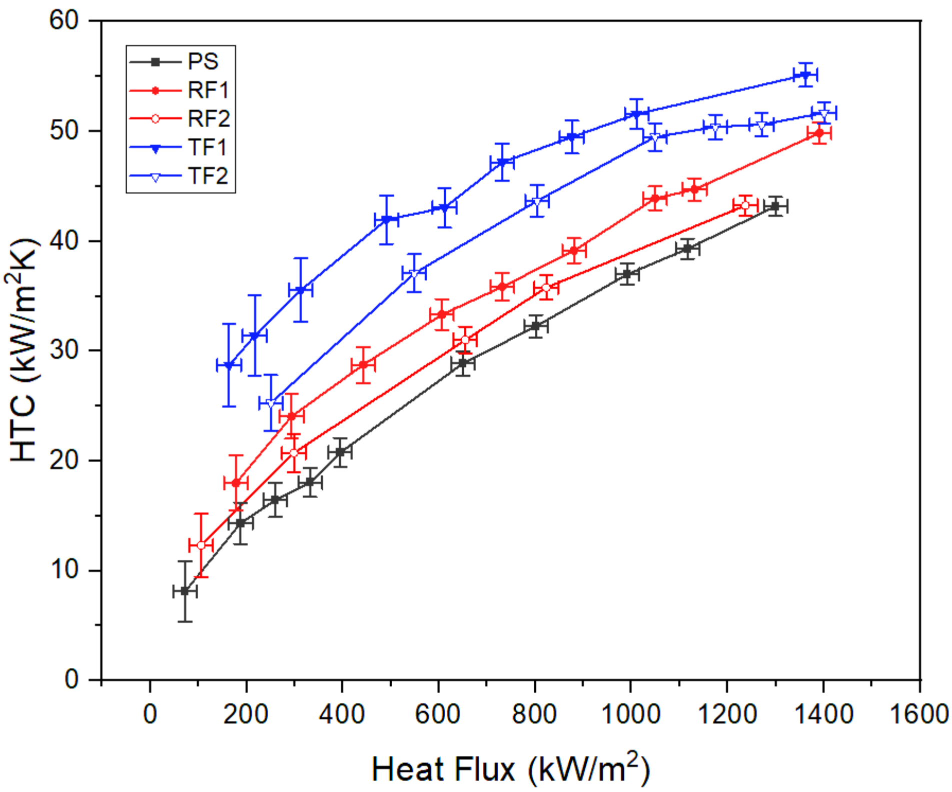

Fig. 18. HTC vs Heat Flux for Test Surfaces with different fin spacing.
(RF1 spacing = 2.14mm, RF2 spacing = 2.54mm, TF1 spacing= 1.6mm, TF2 spacing= 2mm)

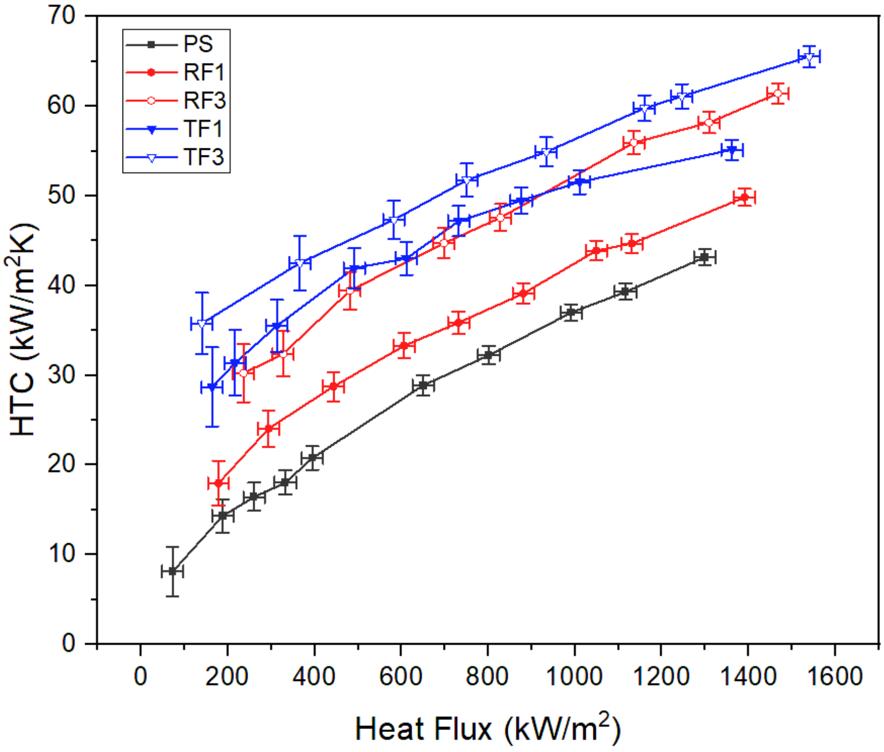

Fig. 19. HTC vs Heat Flux for Test surface with a different fin height
(RF1 ht.=1mm, RF3 ht.= 2mm, TF1 ht.=1mm, TF3 ht. = 2mm)

3.2 Numerical Results

3.2.1 Mesh Independent Study

A mesh-independent study is carried out for all the cases to check the mesh sensitivity of present numerical results. In the case of the plain test surface, we performed simulations at a wall superheat of 15.79K for three structured grids with different cell spacing in the x and y–direction, which is mentioned in Table 3. We observed that the relative change in the heat flux value is less than 1%. Similarly, we performed three simulations for the rectangular and trapezoidal finned test surfaces at wall superheat of 16K and 15.5K and the results are shown in Table 3. To maintain the balance between accuracy and computational time, we selected Mesh No. 1 for both the plain test surface and the trapezoidal finned test surface, whereas Mesh No. 2 is selected for the rectangular finned test surface.

Table 3. Mesh Independent test for three test surfaces

Test Surface	Wall Superheat (K)	Mesh No.	Δx (mm)	Δy (mm)	Change in Results (%)
PS	15.79	1	2.31	1.67	-
		2	1.35	1.35	0.050
		3	1.11	1.11	0.055
RF1	16	1	1.96	1.87	-
		2	1.92	1.5	0.045
		3	1.28	1.21	0.019
TF1	15.5	1	1.5	1.6	-
		2	1.28	1.29	0.071
		3	1.05	1.05	0.026

3.2.2 Assessment of Prediction Capabilities of the Numerical Model

The numerical results of the plain, rectangular finned, and trapezoidal finned test surfaces are compared with the experimental results given in section 3.1. Figure 20 shows the numerical results obtained for different test surfaces. Numerical simulations were performed for plain, rectangular finned and trapezoidal finned test surfaces with default ANSYS FLUENT settings. Here, the RPI wall boiling model with C_w value of 1 is used to estimate the test surface heat flux value. In the numerical simulation, we observed the transient behaviour of the pool boiling and monitored the total heat flux value at the test surface. Simulations were run until a steady state was reached for a particular wall superheat temperature and the average heat flux value over 2s of flow time was considered. From Fig. 20(a), we can observe that the present numerical results reported a larger deviation from the experimental result at lower wall superheat whereas at higher wall superheat difference between numerical and experimental results decreases. This deviation indicates that the default RPI boiling model is inadequate in providing practical results. Different closure models are involved in the RPI boiling model, like drag, lift, wall lubrication, turbulent dispersion models, etc. An investigation of different models is performed to find the most influential interfacial model.

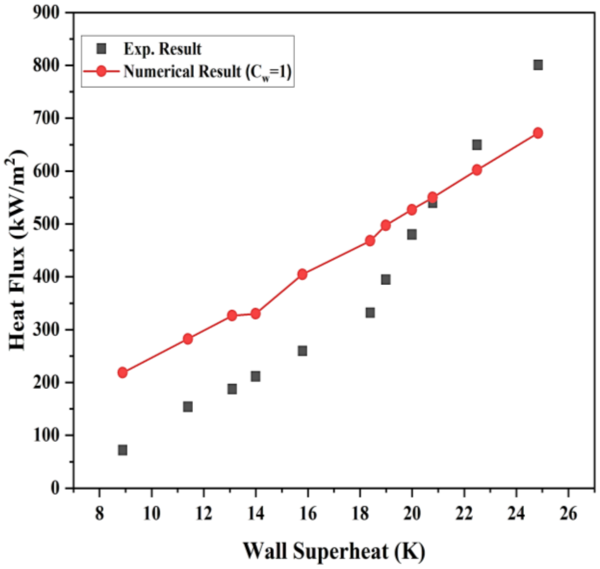

(a)

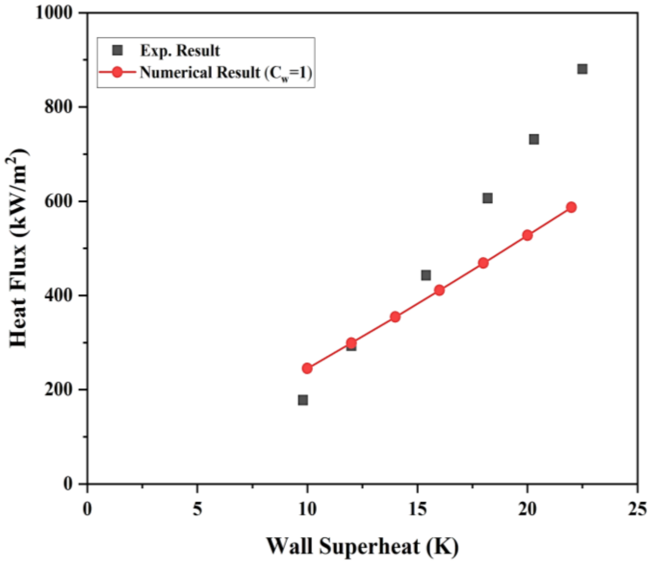

(b)

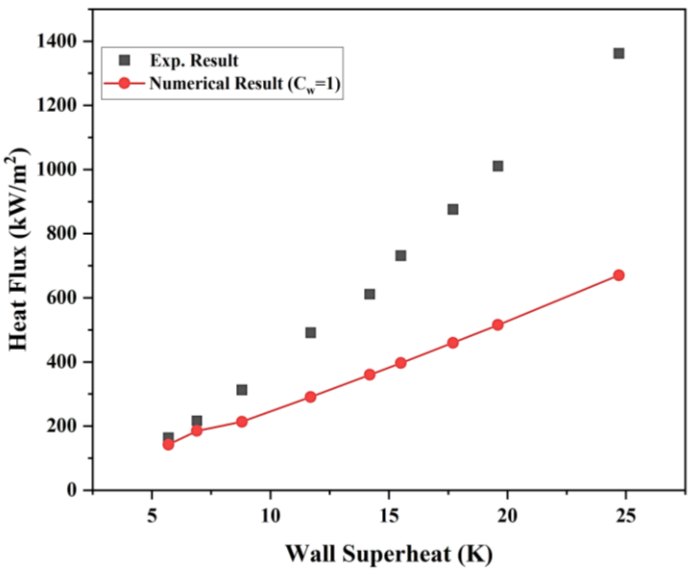

(c)

Fig. 20. Numerical Results (a) Plain Test Surface (b) Rectangular Finned test Surface (c) Trapezoidal Finned test Surface

3.2.3 Influence of Model Closure Equations on the Prediction Capabilities of Numerical Model

3.2.3.1 Effect of Drag Force Models

The liquid–vapour phase interaction induces drag force in the pool boiling process. The drag force between two phases depends on factors like relative Reynolds number, surface tension between different phases, density of phases and bubble diameter. To check the influence of drag models on the numerical results of pool boiling, different drag models are employed one by one. Models considered for the study are the Ishii, Schiller Naumann, Grace et al., and Ishii-Zuber models. The performance of different models is compared with experimental results, as shown in Fig. 21(a). However, no significant improvement is recorded in the numerical results of these drag models. This signifies that further investigation is required to improve the numerical results.

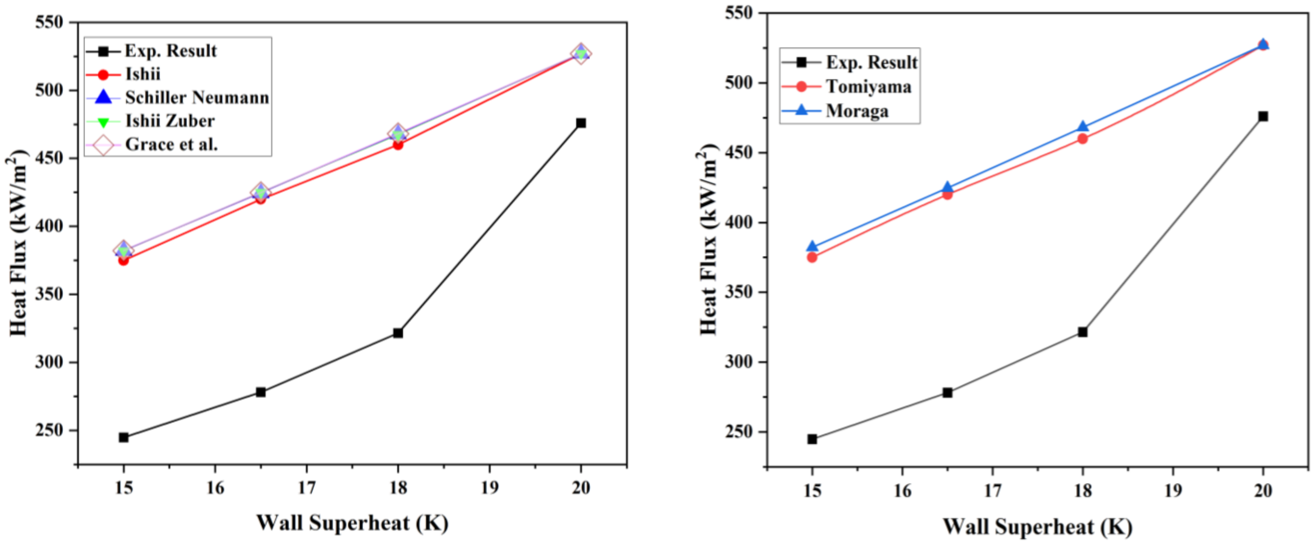

(a) (b)

Fig. 21. Comparison of Numerical Results with Experimental Pool Boiling Result for (a) different drag force models, (b) different lift force models

3.2.3.2 Effect of Lift Force Models

In a multiphase problem, lift force acts on the dispersed phase due to velocity gradients in the continuous phase. The magnitude of lift force depends on the bubble diameter, the density of the primary phase of fluid and the relative velocity between the dispersed phase and continuous phase. To investigate the effect of lift force on numerical results Moraga and Tomiyama lift force model is used. Both these models apply to spherical and ellipsoidal bubbles, respectively. Figure 21(b) compares the outcome obtained using different lift models with the experimental results. It is observed that numerical simulation overpredicts the experimental results in both cases. It may be concluded that lift force models have no significant effect on the numerical results of the pool boiling process.

3.2.3.3 Effect of Wall Lubrication Force Models

The wall lubrication force acts on the dispersed phase to move it away from the heated walls. Antal et al. model, Tomiyama model and Hosokawa model are used to study the effect of wall lubrication force on the numerical results. The results of the Tomiyama and Hosokawa models coincide with each other and the results of these models predict higher heat flux values at corresponding wall superheat when compared to the results of the Antal et al. model. Figure 22(a) shows the pool boiling curve for both experimental and numerical study. The Tomiyama and Hosokawa model results deviate much more from the experimental results, rather than improving on the Antal et al. model of wall lubrication force.

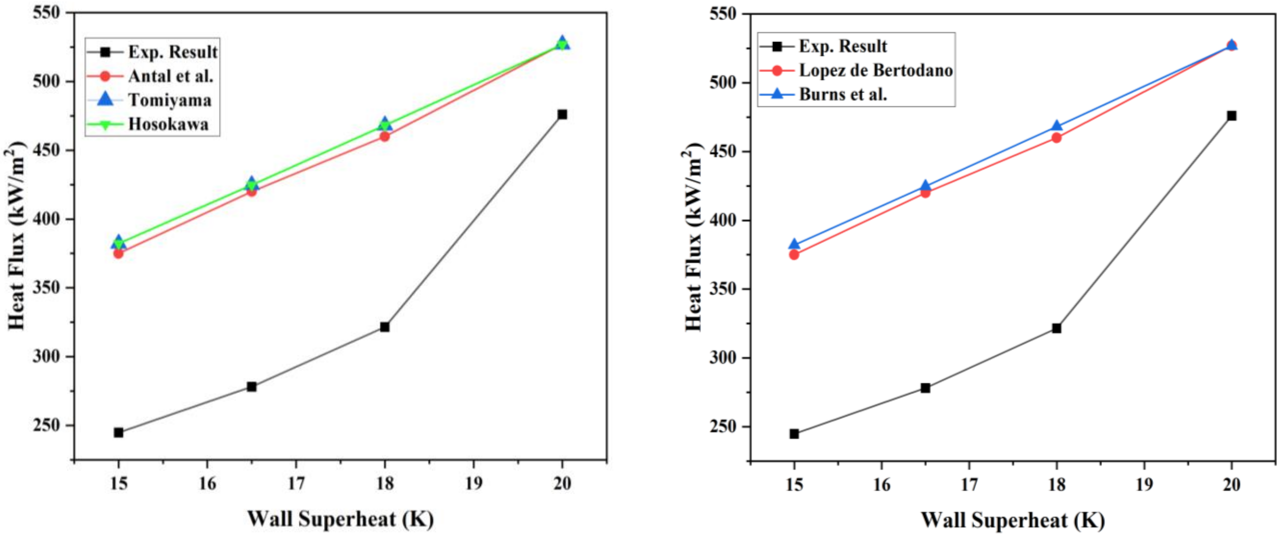

(a) (b)

Fig. 22. Comparison of Numerical Results with Experimental Pool Boiling Result for (a) different wall lubrication force models, (b) different turbulent dispersion force models

3.2.3.4 Effect of Turbulent Dispersion Force Models

In the Eulerian multiphase model, turbulent dispersion force accounts for interphase momentum transfer and helps to move vapour bubbles away from walls in the pool boiling process. The turbulent dispersion force can be modelled using Lopez de Bertadano and Burns et al. models. It depends on the density of the continuous phase, the volume of fraction of dispersed phase and viscosity due to turbulence. The results obtained after using different turbulence dispersion models are shown in Fig. 22(b). It is observed that no significant change is recorded for the numerical results with other turbulent dispersion models and still, there is a deviation between numerical and experimental results.

3.2.3.5 Effect of Turbulence Interaction Models

The turbulence induced by the dispersed phase within the continuous phase is modelled using turbulent interaction models. Troshko-Hassan and Sato models are employed to check the sensitivity of numerical results with turbulence interaction models. Figure 23(a) compares the numerical results of these models against experimental results. The numerical results of both models overpredict the heat flux values at a given wall superheat compared to the experimental results of the pool boiling process.

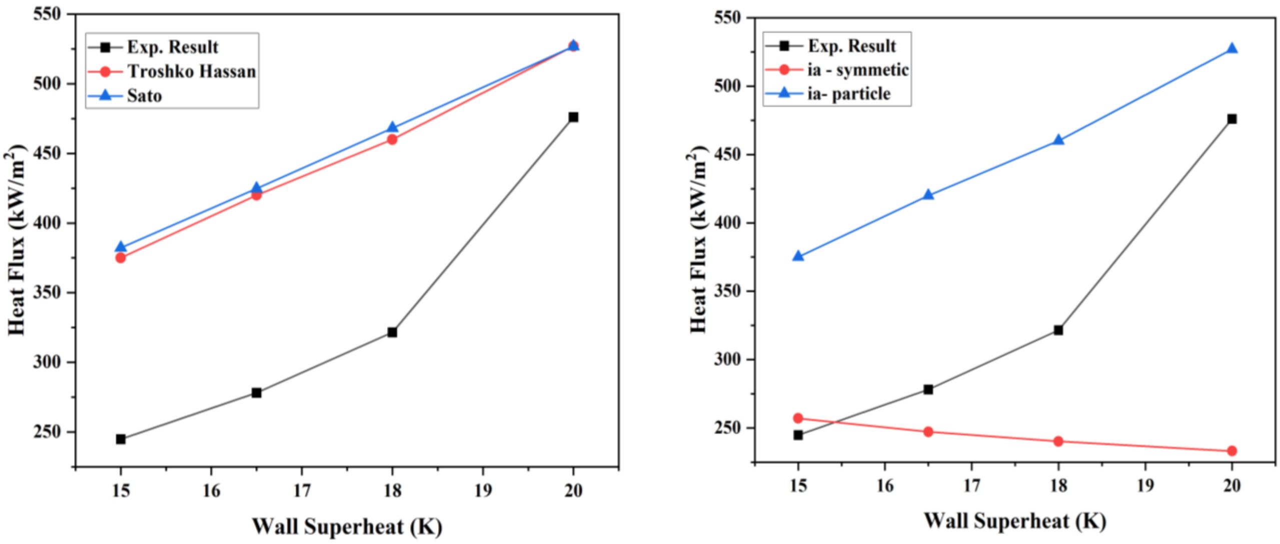

(a) (b)

Fig. 23. Comparison of Numerical Results with Experimental Pool Boiling Results for (a) different turbulent interaction models, (b) different interfacial area concentration models

3.2.3.6 Effect of Interfacial Area Concentration Models

Interfacial area concentration defines the interfacial area between two phases per unit mixture volume in the pool boiling process. It helps to calculate the mass, momentum, and energy transfer through the interface between two phases. The value of interfacial area concentration depends on factors like bubble diameter and volume fraction of the dispersed phase. The numerical results obtained after using the ia-symmetric and ia-particle models are shown in Fig. 23(b). The result of the ia-symmetric model deviates from the experimental result as the wall superheat values increase and it tends to underpredict the heat flux values compared to experimental results. From the figure, it is clear that there is no significant improvement in the numerical results with the application of different interfacial area concentration models.

3.2.4 Identification of influential heat transfer model

We can observe that for all the test surfaces, the numerical results either overpredict or underpredict the experimental results. This clearly shows that there is a need for improvement in one or more parameters of the RPI wall boiling model. RPI considered the heat flux partitioning model for heat transfer where most of the heat transfer occurred through evaporative heat flux and quenching heat flux in the nucleate boiling region. To determine the contribution of different heat fluxes to total heat flux we calculate the proportion of quenching heat flux and evaporative heat flux in total heat flux, which is given in Fig. 24. The figure clearly illustrates that quenching heat flux contribution is much more than that of evaporative heat flux. Similar results were obtained by Kamel et al. (2020), and it was suggested to improve the quenching heat flux value. The RPI boiling model predicts the pool boiling of pure water in two forms: the classical RPI model using the default value of bubble waiting time coefficient (C_w= 1), and the extended RPI boiling model through correcting the quenching heat flux part using a modified bubble waiting time coefficient C_w.

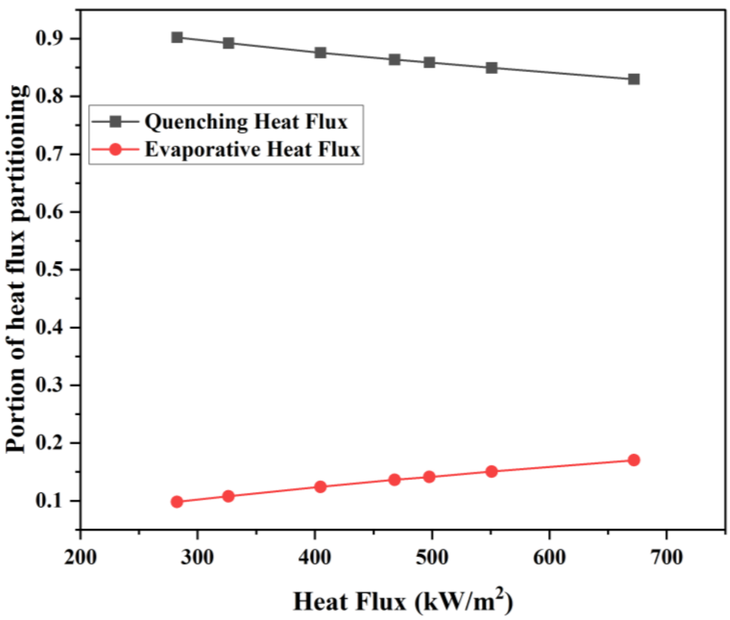

Fig. 24. Fractions of Heat Flux Components

3.2.5 Correlation for Quenching Bubble Wating Time Coefficient

As mentioned in the previous section, the HFP model depends on quenching heat flux, which is the cyclic averaged transient energy transfer associated with the fluid filling on the wall vicinity after the bubble detachment within a certain period. Therefore, the bubble waiting time coefficient Cw is corrected to modify the quenching heat flux model under the RPI boiling model by fitting the experimental data of distilled water. To find the appropriate correlation for the correction of the C_w coefficient, a few simulations are run by changing the C_w value at a particular wall superheat so that the numerical result matches the experimental result. By trial and error, an optimum value of C_w is found for a particular value of wall superheat. A polynomial function is found to be the best fitting for those data in Fig. 25.

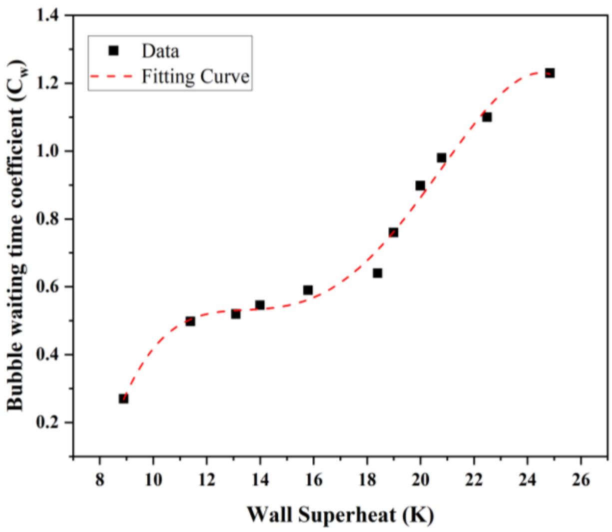

(a)

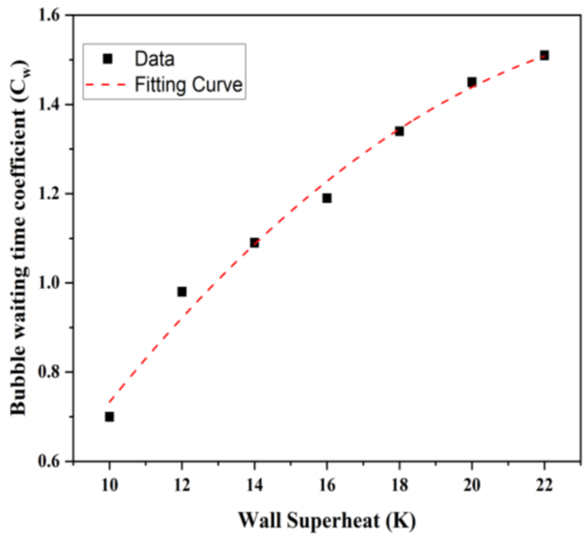

(b)

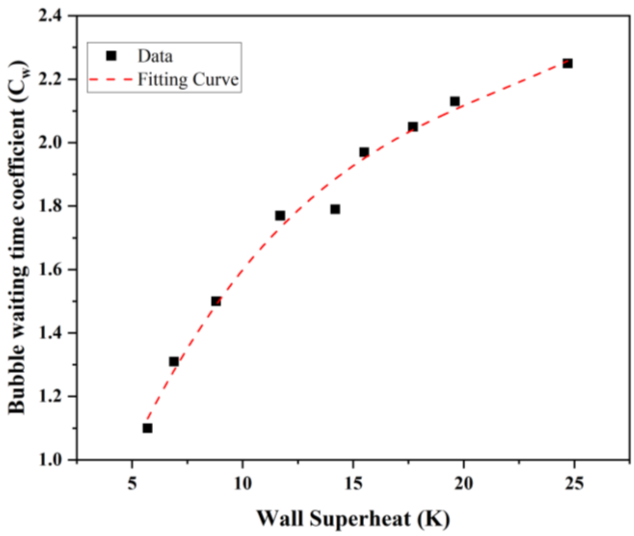

(c)

Fig. 25. Fitting curve for C_w (a) Plain Test Surface, (b) Rectangular Finned Test Surface, (c)Trapezoidal Finned Test Surface

A polynomial function of 4th order is the best fit for the plain test surface with (R^2 =0.9899) as shown Ein q. (32) and a polynomial function of 2nd order is found to be the best fit for rectangular finned test surface with (R^2 =0.9875) as shown in Eq. (33). In the case of the trapezoidal finned test surface, 3rd order polynomial function is the best fit for bubble waiting time coefficient ($R^2 = 0.9888$) data and expression is given in Eq. (34).

$$C_w = -1.3447 * 10^{-4} * (\Delta T)^4 + 0.0092 * (\Delta T)^3 - 0.2256 * (\Delta T)^2 + 2.3834 * \Delta T - 8.7333 \quad (32)$$

$$C_w = -0.0030 * (\Delta T)^2 + 0.1599 * (\Delta T) - 0.5686 \quad (33)$$

$$C_w = 0.0001 * (\Delta T)^3 - 0.0087 * (\Delta T)^2 + 0.2212 * (\Delta T) + 0.1281 \quad (34)$$

Where C_w is the quenching bubble waiting time coefficient, ΔT is wall superheat (K).

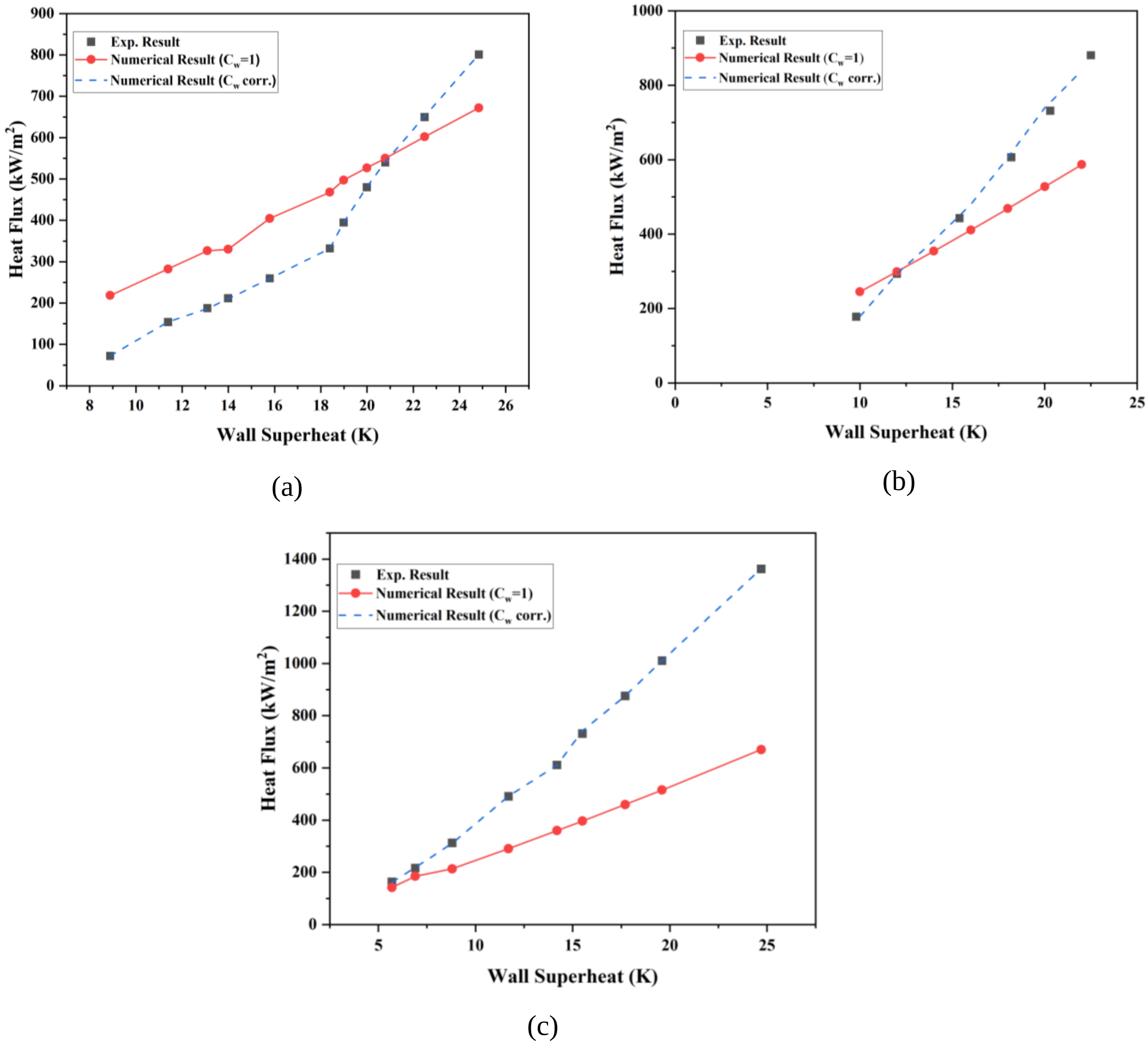

Fig. 26. Numerical Results with Corrected C_w of (a) Plain Test Surface, (b) Rectangular Finned Test Surface, (c) Trapezoidal Test Surface

After calculating C_w value from these correlations, we input these values in the mass interaction model of the RPI model and the results obtained from simulations are given in Fig. 26. The numerical results seem to be in good agreement with experimental data for the boiling curve with the corrected value of C_w, while the model with the default value of this C_w was mainly over predicting the experimental data.

3 CONCLUSIONS

Boiling heat transfer plays a significant role in transporting heat from one medium to another in many heat exchange systems. As one of the most efficient boiling heat transfer regimes, nucleate boiling is involved in numerous industrial applications to remove high heat flux at relatively small wall superheat, making these systems more durable and efficient. Therefore, the enhancement of boiling heat transfer performance has been the subject of numerous studies from the past century. It is wieldy reported in the literature that boiling heat transfer is a complicated phenomenon even for the boiling of pure liquids. In this work, we investigated pool boiling heat transfer experimentally and numerically for different surfaces. The default RPI wall boiling model cannot provide realistic results of pool boiling heat transfer. So, improvements are required to get results similar to experimental results. Here we tried to propose a correlation for the quenching bubble waiting time coefficient (C_w) as a function of the wall superheat. Conclusions which can be drawn from this study are mentioned below:

- The pool boiling performance of the finned test surfaces was better compared to the plain test surface. Heat flux enhancement of 52.3% and 101.5% was observed for the rectangular and trapezoidal finned surfaces.
- The surfaces with higher fin spacing witnessed a reduction in heat transfer due to the formation of discrete bubbles of smaller size and reduced the amount of heat carried away by a single bubble. RF2 and TF2 test surfaces had a heat flux reduction of 27% and 24%, respectively, compared to surfaces with smaller fin spacing (RF1 and TF1)
- Raising the fin height improves heat transfer during the pool boiling process. Because the fins are taller, more surface is available for bubble nucleation and convective heat transfer. However, raising the fin height is not always advantageous because it increases the restriction to bubble motion. Surfaces with increased fin height, RF3 and TF3, performed better in the present work.
- The HTC also improved with the use of the finned test surfaces. HTC is proportional to the area available for heat transfer and depends on the geometry of the test surface.
- The default Eulerian-RPI boiling model was inadequate to get practical results. But the numerical results obtained after correcting C_w value were in good agreement with experimental results.

- For the test surfaces PS, RF1, and TF1, polynomial correlations of C_w as a function of wall superheat were proposed, with the order of polynomial correlation being fourth order, second order, and third order, respectively.

REFERENCES

[1] Avdhoot Walunj, A. Sathyabhama, Comparative study of pool boiling heat transfer from various microchannel geometries, Applied Thermal Engineering, 128 (2018) 672-683.

[2] Barthau G., Active nucleation site density and pool boiling heat transfer-an experimental study, International Journal of Heat and Mass Transfer, 35(2) (1992) 271-278,

[3] Chih Kuang Yu, Ding Chong Lu, Pool boiling heat transfer on horizontal rectangular fin array in saturated FC-72, International Journal of Heat and Mass Transfer, 50(17–18) (2007) 3624-3637.

[4] Enjadat, Suleiman MJ., CFD Comparison of multiphase models in the pool boiling state, Curved and Layered Structures, 9(1), (2022), 382-389.

[5] Esteban Guerrero, Felipe Muñoz1 and Nicolás Ratkovich, Comparison between Eulerian and VOF models for two-phase flow assessment in vertical pipes, Journal of oil, gas and alternative energy sources, (2017).

[6] Farshad Panahizadeh, Mahdi Hamzehei, Mahmood Farzaneh-Gord and Alvaro Antonio Ochoa Villaa, Numerical study on heat and mass transfer behavior of pool boiling in LiBr/H_2O absorption chiller generator considering different tube surfaces, Thermal Science, 25(2B) (2021) 1599-1610.

[7] Hantao Jiang, Nian Xu, Dongdong Wang, Xinyu Yu, Huaqiang Chu, Experimental investigation of the effect of cylindrical array structure on heat transfer performance during nucleate boiling, International Journal of Heat and Mass Transfer, 174 (2021) 121319

[8] Hasan Alimoradi, Sohrab Zaboli, and Mehrzad Shams, Numerical simulation of surface vibration effects on improvement of pool boiling heat transfer characteristics of nanofluid, Korean J. Chem. Eng., 39(1) (2021) 69-85.

[9] M. Feroskhan, T. Venugopal, Naif Mana Almakayeel, T.M. Yunus Khan, Shaik Dawood Abdul Khadar, N. Gobinath, Effect of Thermophoresis on Heat Diffusion in Isobutane/Copper-Oxide Nanofluid under Pool Boiling Condition: Numerical Investigation, Journal of Nanomaterials, vol. 2022, Article ID 2216513, (2022).

[10] Mohammed Saad Kamel, Mohamed Sobhi Al-agha, Ferenc Lezsovits, Omid Mahian, Simulation of pool boiling of nanofluids by using Eulerian multiphase model, Journal of Thermal Analysis and Calorimetry,142: (2020) 493–505.
[11] Montoya, Gustavo; Sanyal, Jay; Braun, Markus; Azhar, Mohammed, On the assessment, implementation, validation, and verification of drag and lift forces in gas–liquid applications for the CFD codes FLUENT and CFX, Experimental and Computational Multiphase Flow, 1(4) (2019) 255–270.
[12] Peter Hübner; Wolfgang Künstler, Pool boiling heat transfer at finned tubes: influence of surface roughness and shape of the fins, 20(8) (1997) 575-582.
[13] Shiro Nukiyama, The maximum and minimum values of the heat Q transmitted from metal to boiling water under atmospheric pressure, International Journal of Heat and Mass Transfer, 9(12) (1966) 1419-1433.
[14] Salehi H. and Hormozi F., Numerical study of silica-water based nanofluid nucleate pool boiling by two-phase Eulerian scheme, Heat Mass Transfer (2018) 54:773–784.
[15] Vishal V. Nirgude, Santosh K. Sahu, Enhancement of nucleate boiling heat transfer using structured surfaces, Chemical Engineering and Processing: Process Intensification, 122 (2017) 222-234.
[16] Wei Li, Renkun Dai, Min Zeng, Qiuwang Wang, Review of two types of surface modification on pool boiling enhancement: Passive and active, Renewable and Sustainable Energy Reviews, 130 (2020) 109926.

[17] Jiansheng Wang, Mengzhen Diao, Xueling Liu, Numerical simulation of pool boiling with special heated surfaces, International Journal of Heat and Mass Transfer, 130 (2019) 460-468.

[18] Yonghai Zhang, Xiang Ma, Jie Zhou, Zeyang Lei, Jinjia Wei, Experimental investigation of pool boiling heat transfer on the radial micro-pillar surfaces, Applied Thermal Engineering, Volume 214 (2022) 118843, ISSN 1359-4311.

[19] Yonghai Zhang, Xiang Ma, Jinyu Wang, Wanbo Liu, Jinjia Wei, Pool boiling heat transfer enhancement on the hybrid surfaces coupling capillary wick and minichannels, International Journal of Heat and Mass Transfer, Volume 203 (2023) 123804, ISSN 0017-9310.
[20] Zhongchao Zhao, Jiaojiao Zhang, Dandan Jia, Kai Zhao, Xiao Zhang, Pengpeng Jiang, Thermal performance analysis of pool boiling on an enhanced surface modified by the combination of microstructures and wetting properties, Applied Thermal Engineering, 117 (2017) 417-426.

[21] Zhang Xiaobin, XIONG Wei, Chen Jianye, Wang Yuchen, K. Tang, CFD simulations and experimental verification on nucleate pool boiling of liquid nitrogen, 25th International Cryogenic Engineering Conference and the International Cryogenic Materials Conference in 2014, ICEC 25–ICMC 2014, (2015).